



**Politecnico
di Torino**

Politecnico di Torino

Master's degree in Electronic Engineering

**Evaluation of a 3D-printing
electrically conductive material
for energy storage devices
fabrication**

Supervisor:
Scaltrito Luciano
Ferrero Sergio
Bertana Valentina

Candidate:
Ge Limeng

April 2022

Abstract

3D printing, also known as Additive Manufacturing (AM), is a revolution in manufacturing techniques based on layer-by-layer fabrication. Thanks to its flexibility, such a technique finds application in different areas. Stereolithography is probably the most consolidated 3D printing technology; it was developed in the 1970s and it is based on the curing of a photosensitive blend (namely resin) by laser-scanning. The resin can be structural or functional. The present thesis work is set in the context of the study of a functional resin (electrically conductive) for stereolithography, which was developed in previous works. The printable material is obtained by mixing PEDOT: PSS particles, which is the intrinsically conductive polymer, as a filler with PEGDA matrix and photoinitiator. In this work, a 3D interdigitated supercapacitor was designed, manufactured, and tested to explore the application of this material in the energy field. The final device consists of an alumina substrate, on which the stereolithography 3D-printed supercapacitor is fixed and enclosed in a silicone chamber. For testing purposes, the chamber was filled with the PVA KCl electrolyte. In the end, the device achieved a good capacity of 19.45 mF/cm^2 with $5 \text{ } \mu\text{A/cm}^2$ current density in the Charge Discharge Galvanostatic test. The electrically conductive resin revealed good capacity retention of 92% after 500 cycles with $10 \text{ } \mu\text{A/cm}^2$ current density charge-discharge.

Contents

List of tables.....	IV
List of figures.....	V
1 Introduction.....	1
1.1 Stereolithography	3
1.1.1 Development.....	3
1.1.2 Process	4
1.2 Polymers for 3D printing.....	6
1.3 Supercapacitor	8
1.3.1 Fundamental.....	8
1.3.2 3D Supercapacitor.....	10
2 Materials and Methods.....	13
2.1 Resin preparation.....	13
2.1.1 Resin composition.....	13
2.1.2 PEDOT filler preparation.....	13
2.1.3 PEGDA matrix preparation.....	15
2.1.4 Stereolithography Resin Preparation	15
2.2 Supercapacitor Fabrication.....	18
2.2.1 Design of Supercapacitor	18
2.2.2 3D Printing Electrodes	19
2.2.3 Assembly of supercapacitor	25
2.2.4 Testing of supercapacitor	28
3 Results and Conclusions	38
3.1 Results data analysis.....	38
3.1.1 0.7mm thickness electrode device	38
3.1.2 1.1mm thickness electrode cell	41
3.1.3 1.3mm thickness electrode cell	42
3.1.4 2.1mm thickness electrode cell	43

3.1.5	Comparison.....	45
3.1.6	Cycling stability.....	47
3.2	Conclusion.....	48
4	References.....	49

List of tables

Table 1 Capacitance and specific capacitance of 0.7mm thickness devices in CCCD measurement at $5\mu\text{A}/\text{cm}^2$ current density.	38
Table 2 Capacitance and specific capacitance of 1.1mm thickness devices in CCCD measurement at $5\mu\text{A}/\text{cm}^2$ current density.	41
Table 3 Capacitance and specific capacitance of 1.3mm thickness devices in CCCD measurement at $5\mu\text{A}/\text{cm}^2$ current density.	42
Table 4 Capacitance and specific capacitance of 2.1mm thickness devices in CCCD measurement at $5\mu\text{A}/\text{cm}^2$ current density.	44
Table 5 Capacitance and specific capacitance of maximum values from 4 different thickness devices.....	45

List of figures

Figure 1 Hull’s stereolithography system[7].....	4
Figure 2 The process flow diagram of stereolithography	6
Figure 3 Ions’ migration at discharge and charge in EDLC[48].....	10
Figure 4 3D printed electrodes: (a) reduced graphene oxide electrodes printed through direct ink writing;[49] (b) graphene/PANI printed electrodes;[50] (c) V2O5/GO and G-VNQDs/GO electrodes and PVA electrolyte are all printed by direct ink writing;[51] (d) PPy deposited Ti5Al4V electrodes printed by selective laser melting.[52]	11
Figure 5 In a H ₂ SO ₄ treatment, the amorphous PEDOT:PSS grains reform into crystalline PEDOT:PSS nanofibrils through a charge-separated transition mechanism.[53].....	14
Figure 6 onductivity of the PEGDA: PEDOT sample at different treated PEDOT:PSS concentration.	16
Figure 7 Conductivity of the PEGDA:PEDOT samples in previous Scordo et al. work but the samples were cured in mold by UV light. [56].....	17
Figure 8 (a) hard mask for sputtering process; (b) 3D structure of supercapacitor. In green and blue the electrodes, in grey the enclosure, in red the platinum connections	18
Figure 9 (a) Microla stereolithography printer, (b) the platform in Microla printer, (c) the adjustable recoater.	20
Figure 10 The software control panel of Microla printer.....	21
Figure 11 (a)The interface of BeamConstruct, (b) Hatch settings, (c) Pen settings	22
Figure 12 Spot light source LC8 used in our work (right one with single lamp).	23
Figure 13 Printed electrode and electrodes in 0.7mm, 1.1mm, 2.1mm thickness.	24

Figure 14 One couple of electrodes shows the deformation may cause a short circuit between two electrodes.....	24
Figure 15 Assembly process of supercapacitor: (a) Etched alumina substrate; (b) Alumina substrate after sputter the platinum current collector; (c) inlay and glue electrodes and silicone chamber; (d) Enclosed cell with two holes for electrolyte injection.....	25
Figure 16 A close looking of etched alumina substrate.	26
Figure 17 PVA/KCl electrolyte.....	28
Figure 18 Key performance metrics, test methods and affecting factors for supercapacitors[59].....	29
Figure 19 CV plot of ideal double layer capacitor, resistive capacitor and pseudocapacitor.[60].....	30
Figure 20 The equivalent circuit models introduced by Boonpakdee et al. to analysis the CV plot.[61].....	31
Figure 21 CCCD curve of a supercapacitor.[59].....	33
Figure 22 A general Nyquist plot for an electrical double layer capacitor.[62]...	35
Figure 23 (a) two-electrode system; (b) three-electrode system.....	36
Figure 24 (a) a cell is connected to the instrument by two micromanipulators; (b) a close looking of the probes are touched to the platinum current collector.	37
Figure 25 CV plot (left) at 1mV/s, 2mV/s, 5mV/s, and 10mV/s scan rates, and CCCD plot (right) at 5 μ A/cm ² , 10 μ A/cm ² , 20 μ A/cm ² , 50 μ A/cm ² of 0.7mm thickness device.	39
Figure 26 0.7mm thickness device Coulombic efficiency (left) and Ragone plot (right) at 5, 10, 2, 50,100, and 200 μ A/cm ²	39
Figure 27 Area-normalized Ragone plots of representative supercapacitor and performance requirement to work in different applications such as energy harvesters, sensors, and wireless communications.[63].....	40

Figure 28 CV plot (left) at 1mV/s, 2mV/s, 5mV/s, and 10mV/s scan rates, and CCCD plot (right) at 5 μ A/cm ² , 10 μ A/cm ² , 20 μ A/cm ² , 50 μ A/cm ² of 1.1mm thickness device.	41
Figure 29 1.1mm thickness device Coulombic efficiency (left) and Ragone plot (right) at 5, 10, 2, 50,100, and 200 μ A/cm ²	42
Figure 30 CV plot (left) at 1mV/s, 2mV/s, 5mV/s, and 10mV/s scan rates, and CCCD plot (right) at 5 μ A/cm ² , 10 μ A/cm ² , 20 μ A/cm ² , 50 μ A/cm ² of 1.3mm thickness device.	43
Figure 31 1.3mm thickness device Coulombic efficiency (left) and Ragone plot (right) at 5, 10, 2, 50,100, and 200 μ A/cm ²	43
Figure 32 CV plot (left) at 1mV/s, 2mV/s, 5mV/s, and 10mV/s scan rates, and CCCD plot (right) at 5 μ A/cm ² , 10 μ A/cm ² , 20 μ A/cm ² , 50 μ A/cm ² of 2.1mm thickness device.	44
Figure 33 2.1mm thickness device Coulombic efficiency (left) and Ragone plot (right) at 5, 10, 2, 50,100, and 200 μ A/cm ²	45
Figure 34 (a) CV plot of 4 different thickness devices at 1mV/s scan rate; (b) CCCD plot of 4 different thickness devices at 5 μ A/cm ² ; (c) Ragone plot of 4 different thickness devices.	46
Figure 35 Capacity retention and Coulombic efficiency in cycling stability test.	47

1 Introduction

3D printing is one kind of rapid prototyping technology, also called Additive Manufacturing (AM). The core idea of Additive Manufacturing (AM) is to pile material layer-by-layer to obtain the object in three-dimensions, which is fundamentally different from traditional Subtractive Manufacturing (SM) which can cause waste of material and often is energy inefficient [1]. Like 2D printer prints one layer of ink on paper, 3D printer creates layer-by-layer three-dimensional objects in from computer assisted design (CAD).[2] Now, 3D printing has been widely used in diverse fields, such as electronics[3], medical industry [4], architecture [5]. Many approaches of 3D printing have been explored, such as Fused Deposition Modeling (FDM), Inkjet Printing (IJP), Selective Laser Sintering (SLS), Three-dimensional Printing (3DP), Stereolithography (SL), etc. [6] In particular, Stereolithography (SL) is one of the most mature technology. The method of stereolithography is accomplished by localized photopolymerization. This process is triggered by ultraviolet (UV) radiation and occurs in a bath filled with liquid monomers, oligomers and photoinitiators.[7] Stereolithography has enough versatility to fabricate different complex 3D geometry with high resolution and acceptable cost [8]: more and more materials [9] have been developed for a wide range of applications, such as sensors [10], tissue engineering[11], microfluidics devices [12] and energy storage components [13].

As regards sensors and energy storage components, the adoption of electrically conductive materials is crucial. An intuitive method to achieve highly electrically conductive polymer composite is to mix conductive fillers into insulating polymer matrix. There are different kind of materials can be used as conductive fillers, such as carbonaceous fillers (carbon[14], carbon nanotubes[15] and graphene[16]), metal nanoparticles and intrinsically conductive polymers[17]. Poly(3,4-

ethylenedioxythiophene) (PEDOT) was first proposed in a patent by Bayer AG in 1988. It was found to have a stable doped structure and has excellent stable electrical conductivity.[18] At the same time, people developed the poly(3,4-ethylenedioxythiophene): poly(4-styrenesulfonate) (PEDOT:PSS) micellar system to achieve the water storage and processing of PEDOT materials, which makes it widely used in energy storage [19], flexible electronics[20], photoelectric conversion devices [21] and other applications. Polyethylene(glycol) diacrylate (PEGDA) is a blank slate hydrogel that polymerizes rapidly at room temperature in the presence of a photoinitiator and UV light. Those characteristics make PEGDA be the perfect host matrix, and treated PEDOT: PSS particles play the role of conductive filler; mixed together, they can lead to an electrically conductive resin for SL. [22]

Supercapacitors, also known as electrochemical capacitors, are electrochemical energy storage devices that store energy through a polarized electrolyte. Differently from the traditional chemical power supply, supercapacitors have special performance between traditional capacitors and batteries. Electrical double layer capacitors (EDLC) are devices that store electrical energy in the electrical double layer that form at the interface between an electrolytic solution and an electronic conductor.[23] No chemical reaction occurs during the energy storage process, and the process is reversible, so EDLCs can be repeatedly charged and discharged hundreds of thousands of times. The outstanding advantages are high power density, short charge and discharge time, long cycle life, and wide operating temperature range.[24] Nowadays, supercapacitors are used in many areas, such as photovoltaic solar systems [25], wind energy conversion systems [26], and electric vehicles [27].

In this thesis, the design and fabrication of a supercapacitor is presented, which electrodes are manufactured by 3D printer (stereolithography) with a new custom formulation of a conductive resin (PEGDA:PEDOT).

1.1 Stereolithography

Stereolithography (SL), which uses laser curing to polymerize successive layers of liquid resin, was the first 3D printing technology available in the market and can be considered the most important rapid prototyping technology currently available.[28]

1.1.1 Development

The first important work related to modern stereolithography additive manufacturing technology appeared in 1970s. Swainson proposed a patent for a system which use intersecting radiation beams to photochemically cross-link a 3D object.[29] Then, Herbert introduced a system that uses photosensitive polymers to build solid objects layer-by-layer.[7] However, Chuck Hull proposed the term “stereolithography” in the patent that he applied in 1984.[30] On the basis of Hull’s idea, liquid state photosensitive material is cured by scanning laser beam layer-by-layer to create 3D solid state objects. In Figure 1, the basic structure of Hull’s stereolithography system is reported.

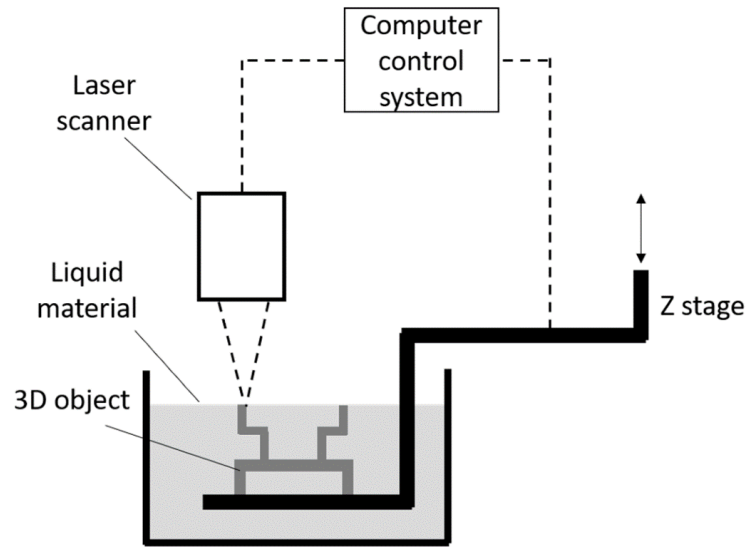


Figure 1 Hull's stereolithography system[7]

After that, the second generation which is called mask-projection stereolithography uses photo mask to cure each layer instead of scanning laser beam. By doing this, it reduces the scanning time and improves the efficiency.[31] In 2015, a new simpler and faster stereolithography is presented which is called Continuous Liquid Interface Production (CLIP), it can be seen as fourth generation.[32] Lastly, the fourth generation can be defined as volumetric stereolithography which can reduce the processing time to few seconds.[33] Moreover, the material type can define a stereolithography process: thus, color stereolithography[34], multi-material stereolithography[35] were developed.

1.1.2 Process

The stereolithography process starts from computer aided design (CAD) programs. From the CAD design, the geometry file can be generated in STL format. STL stands for standard tessellation language. STL was created by the company 3D Systems Inc and

was originally used for stereolithography, but now it is the standard file for every 3D printing process.[36] When the STL file is generated, the designed surfaces and curves will be converted into meshes which consist of a series of triangles. In the laser control software, the geometry in STL will be sliced layer-by-layer into 2D cross sections and the laser scanning path will be calculated and written on the 2D layers. After that, the printing process or the polymerization process will begin. At the beginning, a tank or container is filled with liquid light-curable resin, the working platform is at the same level as the liquid surface. The liquid surface is always at the focus plane of the laser, and the focused spot scans the liquid surface line by line according to the computer instructions, polymerizing the resin line by line. When the scanning of one layer is completed, the platform moves one layer down, and the printed part is covered with a layer of fresh resin. Then a recoater, also called doctor blade, will smooth and uniform the surface of the resin. By repeating these steps, the printing of the object is accomplished. When the manufacturing is finished, the sample will be manually removed from the printer and on other printing can start processed.

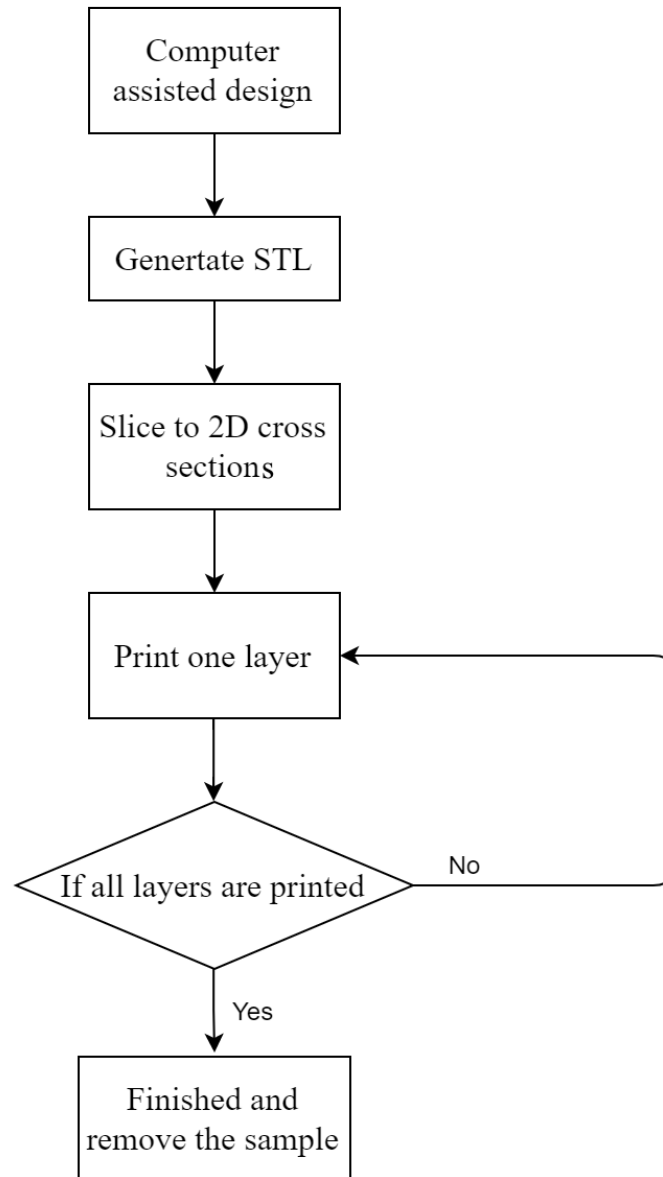


Figure 2 The process flow diagram of stereolithography

1.2 Polymers for 3D printing

Polymers are the most suitable material for AM and can be classified as thermoplastics and thermosets. Then, such polymers can be modified, then polymer matrix composites, particle reinforced polymer composites, fiber-reinforced polymer composites, nanocomposites are defined.[37]

Thermoplastic is one kind of plastic that can be repeatedly melted at high temperatures and solidified after cooling down. AM processes such as, SLS and FDM can build complex components by thermoplastics. For example, a PDMS microfluidic flow chambers can be fabricated by a 3D printed polyvinyl alcohol (PVA) water-soluble mold.[38] A bio-based blend of Polylactic acid (PLA) can be processed by FDM.[39] On the contrary, thermosets are polymers which degrade rather than melting when subjected to thermal treatments.

Polymer matrix composites (PMCs) were introduced to overcome the disadvantages of polymers, such as poor mechanical properties. PMCs typically include various short or continuous fibers combining with organic polymer matrix. For example, carbon fiber can be combined with acrylonitrile styrene acrylate (ASA) to increase flexural Young's modulus and thermal conductivity.[40]

Particle reinforced composites are generally dispersion of particles such as a filler mixed into another material as a matrix. Multi-wall carbo nanotubes (CNTs) coated polyamide 12 powders are developed in SLS process to obtain better heat conduction and heat absorption.[41] In stereolithography, graphene oxide (GO) is mixed to photocrosslinkable resin to achieve a further optimization due to the high shrinking and brittleness of the 3D constructs.[42]

Fiber reinforced polymer composites are composite materials including three elements: fibers, matrix, and interface. Carbon fiber is one of the most used fibers which can improve the compression strength, flexural strength, and flexural stiffness.[43]

Nanocomposites always can be applied to optimize the properties and multifunctionality. In this work, the printable material is obtained by mixing PEDOT: PSS

particles with PEGDA to achieve an electrically conductive resin for more functionality.[22]

Responsive polymers have the capability to change their chemical and physical properties by exposed to different external stimulation such as temperature, pressure, ion concentration, and presence of other molecules. Polyvinyl alcohol (PVOH) is one of the thermal sensitive polymers which can be applied to a pellet-fed melt extrusion technique and can achieve significant mechanical properties and complex structure at certain temperature.[44]

1.3 Supercapacitor

Supercapacitor refers to a type of energy storage device between traditional capacitors and rechargeable batteries. It not only has the characteristics of fast charging and discharging device, but also has the advantage of increased lifetime and cyclability respect to batteries.

1.3.1 Fundamental

In 1853, Helmholtz first described the electric double-layer (EDL) phenomenon. In 1910 and 1913, Gouy and Chapman found that the capacitance is not constant in an EDL. Gouy Chapman model improved the prevailing knowledge of EDL.[45] In 1924, Stern proposed the model that a plate (the Stern layer) separate the double layer, and it made the DEL theory more scientific and complete.[46] In 1947, Grahame proposed that some charged, or electrically neutral particles can go through the stern layer

because pseudocapacitance behaviors.[45] In 1957, Becker (General Electric Company) first patented a double-layer structure with porous carbon material electrodes. In 1971, NEC (Nippon Electric Company) launched commercially successful double-layer capacitors under the name “super capacitor”.[47]

According to different energy storage mechanism, the supercapacitor can be divided into two major categories of the Electric double-layer capacitor (EDLC), Faradaic quasi-capacitor (pseudocapacitor) and Asymmetric or Hybrid capacitor.[48] Among them, the double-layer capacitance is characterized by electrostatic energy storage by separating charges at the interface between the surface of a conductive electrode and an electrolyte without faradaic reactions. In this electrode and electrolyte system, an electrical double layer arises at the electronically conductive electrode and ionically conductive electrolyte solution interface. Pseudocapacitance is characterized by storing electrical energy through fast reversible redox reactions, intercalation, and adsorption at or near the surface of some electrode materials.[48] Pseudocapacitors are generally made of metal oxide or conductive polymer electrodes.

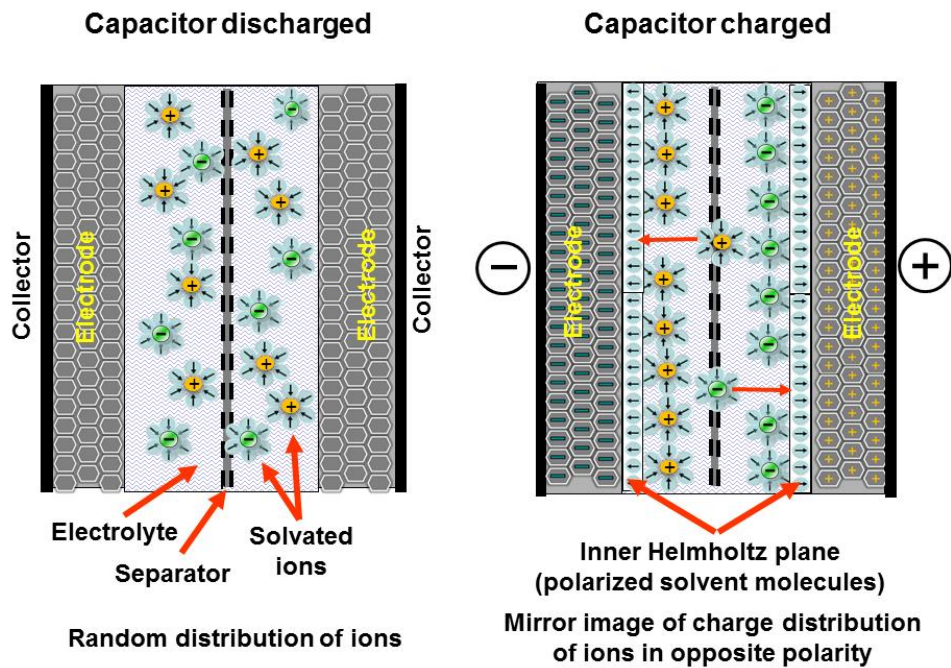


Figure 3 Ions' migration at discharge and charge in EDLC[48]

1.3.2 3D Supercapacitor

One of the main disadvantages of supercapacitors is that the areal capacitance is limited because of the low material load per unit area on the substrate. A three-dimensional (3D) electrode having a high aspect ratio can break out the substrate area limitation and achieve a high capacitor performance. 3D printing technology can provide the functionality to fabricate thick electrodes with high aspect ratio.

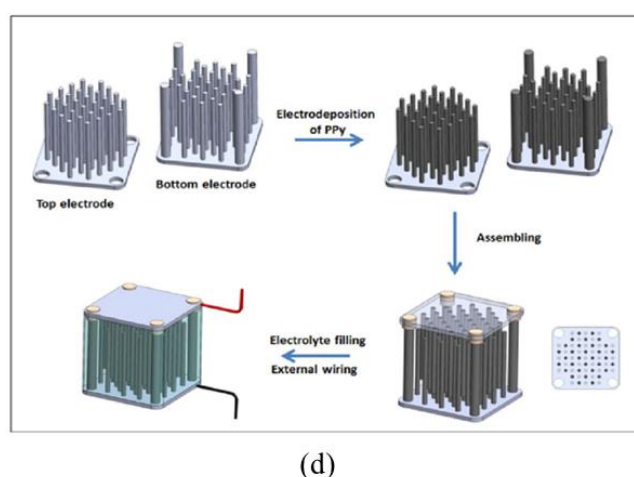
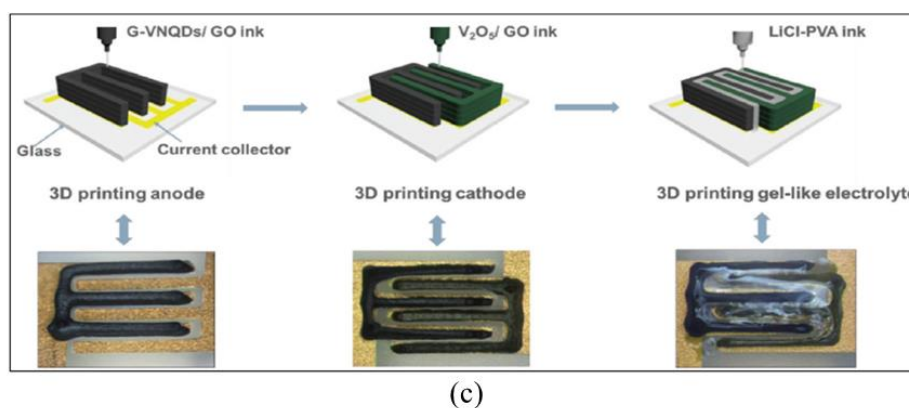
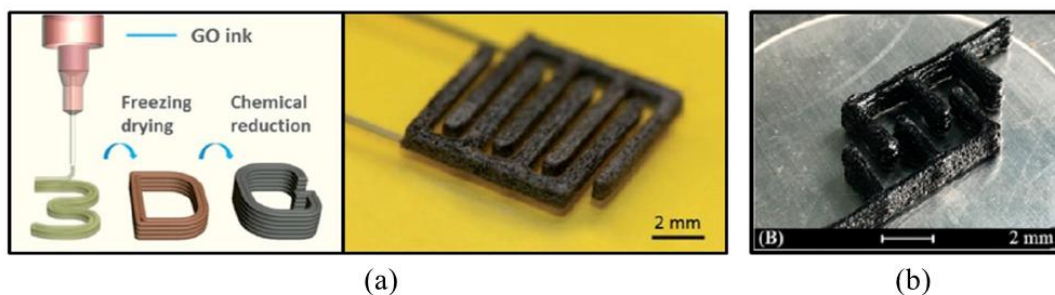


Figure 4 3D printed electrodes: (a) reduced graphene oxide electrodes printed through direct ink writing;[49] (b) graphene/PANI printed electrodes;[50] (c) V₂O₅/GO and G-VNQDs/GO electrodes and PVA electrolyte are all printed by direct ink writing;[51] (d) PPy deposited Ti5Al4V electrodes printed by selective laser melting.[52]

In literature, it is possible to find some examples of 3D printed electrodes. In Figure 4(a)[49], graphene oxide (GO) and DI water ink is printed on Cr/Au current collectors by direct ink writing. The electrodes show a very stable capability since the device

based on these electrodes can retain 100% capacitance retention after 10,000 cycles at 10mV/s. In Figure 4(b)[50], another report of graphene/PANI (Polyaniline) electrodes printed by direct ink writing. This supercapacitor achieved a high areal capacitance of 1329 mF/cm². In Figure 4(c)[51], the 3D printing material consisted of Vanadium pentoxide (V₂O₅) and graphene-vanadium nitride quantum dots (G-VNQDs) with GO. The electrolyte was LiCl in PVA which can also be printed by direct ink writing method. This supercapacitor achieved an areal capacitance of 207.9 mF/cm². In Figure 4(d)[52], are shown 3D printed titanium electrodes. The electrodes were coated with Polypyrrole (PPy) by electrodeposition. This supercapacitor achieved an areal capacitance of 0.057F/ cm² at 20mV/s scan rate and retained 90% and 78% capacitance retention at 500 and 1000 cycles.

3D supercapacitor technology is promising for the development of energy storage devices; however, challenges exist in practical applications. From 2D to 3D architecture electrode design and implementation gains extremely increasing areal capacitance, but the structural complexity of the electrode is limited. The design of electrodes also needs to emphasize the mechanical durability and fabrication ease. The optimization of 3D printing materials is also challenging.

2 Materials and Methods

In this chapter, the 3D printing material preparation, supercapacitor fabrication and testing are presented.

2.1 Resin preparation

2.1.1 Resin composition

Clevios PH 1000, purchased from Heraeus, is an aqueous PEDOT: PSS dispersion. The specific conductivity is up to 1000S/cm. (Electric conductivity: Gold 44.2×10^8 S/cm; Platinum 9.3×10^8 S/cm).

Polyethylene glycol diacrylate (PEGDA) Average Molecular Weight 250, was purchased from Sigma Aldrich.

Irgacure 819, purchased from Sigma Aldrich, is the commercial name for Phenylbis (2,4,6-trimethylbenzoyl) phosphine oxide, also called Bisacylphosphine oxides (BAPOs), which is a versatile UV photoinitiator for radical polymerization of unsaturated resins.

2.1.2 PEDOT filler preparation

In this work, the conductive filler, after it will be also called ‘PEDOT particles’, was obtained from Clevios PH 1000. A treatment to remove the excess of water and enhance the conductivity is needed. Clevios PH 1000 is diluted in 0.5M sulfuric acid. 0.5M H₂SO₄ treatment causes important structural rearrangements in PEDOT:PSS by

partially removing PSS, leading to the formation of crystalline nanofibers through the transition mechanism of charge separation.[53] Since the homogeneous mixture of filler and matrix is affected by the size of PEDOT agglomerates, which also influence the printing accuracy, ethanol was involved to optimize the dispersion of PEDOT agglomerates, because ethanol have low density that helps to suspend them better.[54]

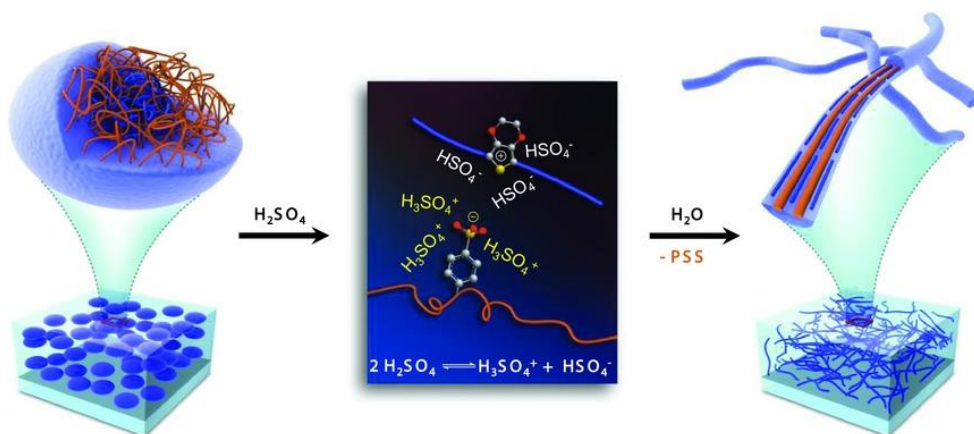


Figure 5 In a H_2SO_4 treatment, the amorphous PEDOT:PSS grains reform into crystalline PEDOT:PSS nanofibrils through a charge-separated transition mechanism.[53]

PEDOT was prepared according to the procedure used by Scordo et al. in 2019.[22] Firstly, 0.5 M sulfuric acid was prepared by diluting 14 ml sulfuric acid in 500ml deionized water. 10 vol.% Clevios PH 1000 was added into the dilution and left it to rest for at least 12 hours. During this time, PEDOT was separated from the solvent, depositing on the bottom of the beaker. Then, supernatant was removed in the middle and put left mixture in 50mL Falcon containers. After supernatant removal, PEDOT was centrifugated at 4000 rpm for 10 minutes in centrifuge (OHAUS, Frontier 5706) to separate the PEDOT agglomerates from sulfuric acid. To obtain smaller PEDOT particles size, a double weight of ethanol was added to the centrifuged blend and left rest overnight. Then, it was subjected to a “grinding” step with Branson sonifier (Branson Ultrasonics Sonifier SFX250 Cell Disruptors) which was set 5 seconds on, 5 seconds off, for total 10 minutes with 70% power. For further reduction of PEDOT particles size, PEDOT in ethanol mixture was processed with Ultra-Turrax (IKA, Ultra-

Turrax dispersers T25) for 20 minutes at speed 4. The final step is to separate the PEDOT agglomerates from the ethanol with centrifuge at 4000 rpm for 14 minutes. The final obtained sample is named treated PEDOT:PSS which is ready to be used.

2.1.3 PEGDA matrix preparation

The photocurable PEGDA 250 plays the role of host matrix in this SL resin. To achieve the light triggered polymerization, small amounts of photoinitiator (Irgacure 819) were mixed with PEGDA.[55]

In this work, the amount of photoinitiator is calculated as percentage of the PEDGA mass used. 1 wt.% of photoinitiator is dissolved in PEGDA with Branson sonifier which is set 5 seconds on, 5 seconds off, for total 15 minutes with 30% power in ice bath.[22]

2.1.4 Stereolithography Resin Preparation

To obtain the 3D printing resin, simply mix the treated PEDOT: PSS and PEGDA with photoinitiator by magnetic stirring at 400 rpm for 10 minutes.

The weight ratio of PEGDA and PEDOT was optimized for stereolithography process and final application. To investigate the electrical conductivity and printability of the resin, different weight ratios were prepared. 10% wt., 15% wt., 25% wt., 35% wt., 45% wt., 52.8% wt. of PEDOT were mixed into PEGDA with respect to the total resin weight. Afterwards, three samples (0.5 x 0.5 x 1 cm³ cuboid) of each weight ratio were printed by stereolithographic 3D printer. To measure the electrical conductivity, the silver

conductive paste was applied on two opposite surfaces of each sample and contacted by means of micromanipulators and probes. The conductivity measurement is performed by I/V measurement. By applying sweeping voltage from -1V to 1V, current was measured. Then, resistance and conductivity were calculated. In Figure 6, the relationship between the conductivity of samples and the percentage of PEDOT in the PEGDA resin is reported.

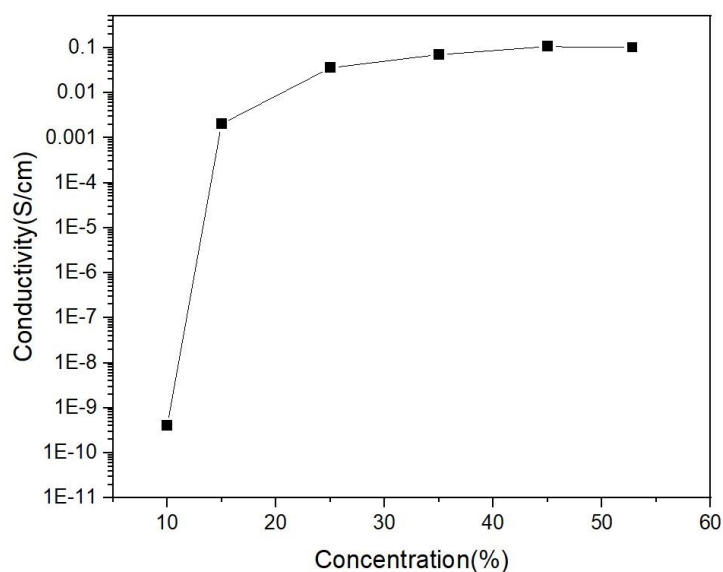


Figure 6 onductivity of the PEGDA: PEDOT sample at different treated PEDOT:PSS concentration.

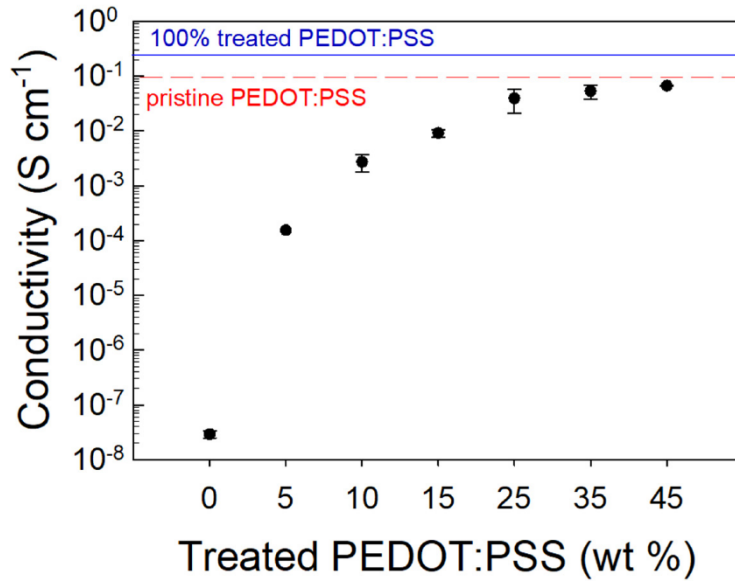


Figure 7 Conductivity of the PEGDA:PEDOT samples in previous Scordo et al. work but the samples were cured in mold by UV light. [56]

From the obtained results, the conductivity of sample is getting higher with the more treated PEDOT:PSS was added to the matrix. Similar result was observed in previous research, as shown in Figure 7.[56] For the filler percentage over 30%, the conductivity of samples has no big difference comparing to low percentage. When the filler percentage exceeds 45%, the printability of the resin is lost due to the high viscosity of the composite material. High viscosity does not allow the liquid resin to be uniformly spread on the SL printer platform.[56] At the meantime, the mechanical characterization gets poor when the concentration of filler increases in the resin. In this work, 35% wt., is chosen as the optimal treated PEDOT:PSS percentage inside the PEGDA matrix.

2.2 Supercapacitor Fabrication

2.2.1 Design of Supercapacitor

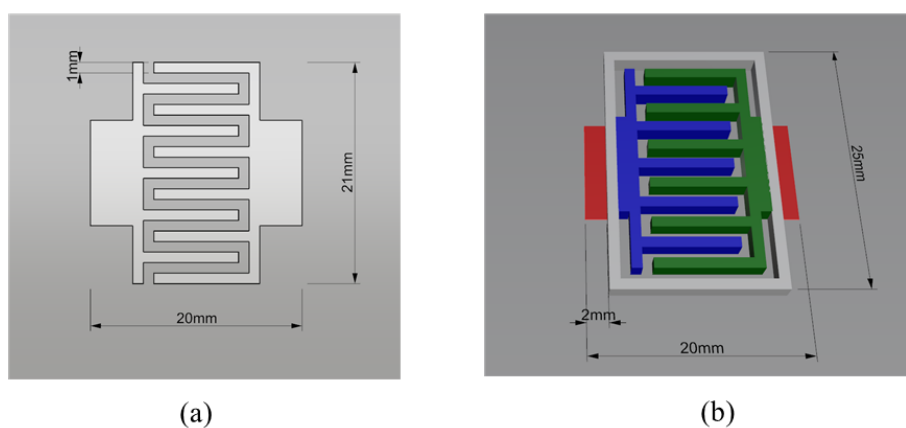


Figure 8 (a) hard mask for sputtering process; (b) 3D structure of supercapacitor. In green and blue the electrodes, in grey the enclosure, in red the platinum connections

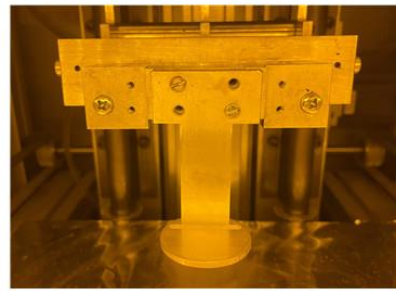
The design of the supercapacitor is based on an interdigitated geometry with 1 mm wide fingers. Such geometry was employed both for electrodes printing and for hard mask Figure 8(a) used for sputtering the current collector. Indeed, the final device will include an insulant substrate on which the 3D printed electrodes are fixed. On the surface of such substrate, a thin metal layer was deposited with the almost the same geometry of the electrodes to obtain the collector. Indeed, the collector includes a 2 mm additional area in order to allow the probes connection during testing. Three electrodes thickness (0.5mm, 1mm and 2mm) will be considered. The enclosing chamber is a 1mm thick and 2mm high wall surrounding the two electrodes and a rectangle cover will be used to seal it and avoid the electrolyte evaporation. As it is shown in Figure 8(b), the two electrodes are blue and green, the chamber is light grey, and two contact pads are reserved for measurement connections are in red.

2.2.2 3D Printing Electrodes

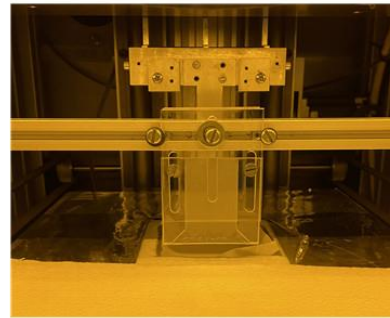
In this work, we used a customized stereolithography 3D printer (Microla Optoelectronics Srl) (Figure 9(a)) which is a laser scanning stereolithography printer which uses a 405nm wavelength laser and can print on a maximum area of 170 x 200 mm². To achieve the laser scanning, the galvo-scanner is involved. Galvo-scanner consists of two galvanometric mirrors which rotate on two vertical spin axes, and it can control the laser beam to scan at X-Y directions.[57] Also, a motorized stage (Figure 9(b)) is needed to move the objects up and down at the right polymerization position. For this printer, after each layer is printed, the platform will go down and dip in and wait for the resin to reflow on it, then it goes up to the recoat level, so the recoater can go back-forward to uniform the resin layer and remove the surplus resin. Then the platform goes down to the laser focus level for the laser to scan the next layer. When the platform moves to recoat level and laser focus level (start level), we need consider the height of objects which were printed, so after each layer the platform will be one layer thickness (in our case, one layer is 100μm) lower than the previous level. In this case, we will always keep the upper surface of our objects at the correct working levels. The recoater (Figure 9(c)) in this printer is adjustable. At the beginning of the printing, we can control the platform to move to recoat level and put different spacers between the recoater and platform to adjust different recoat thicknesses.



(a)



(b)



(c)

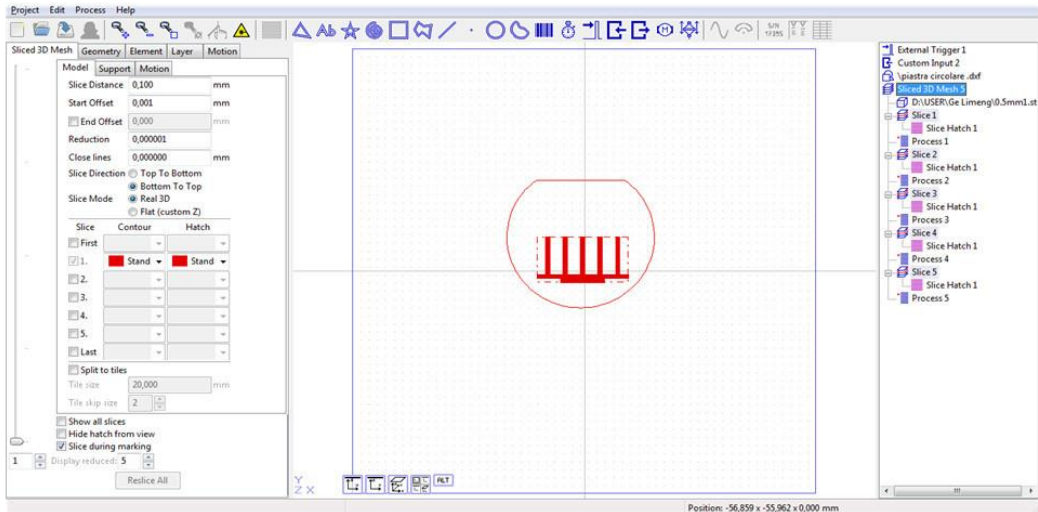
Figure 9 (a) Microla stereolithography printer, (b) the platform in Microla printer, (c) the adjustable recoater.

Figure 10 shows the control panel of Microla 3D printer. On the right side of the panel, there are buttons to start or stop the process and control the platform to go to certain position. 'Go_Racla' can set the platform to recoat position. At this position we can adjust the recoating thickness between platform and recoater. 'Go_Start' can set the platform to the laser focus point level, which is the position laser scanning always working at, so in this position we can fill or remove resin in or out the container to make liquid surface at the same level as the platform. 'Go_Zero' can move the platform to zero position which will give us more space to remove the platform, container to do cleaning. On the right side, we can also enable the laser and control the laser power, which is a very important parameter in printing which is usually set 40 mW in this work. On the left side of the panel, there are two information windows. The upper one shows the printing logs of each step and the certain position the platform will go. The bottom

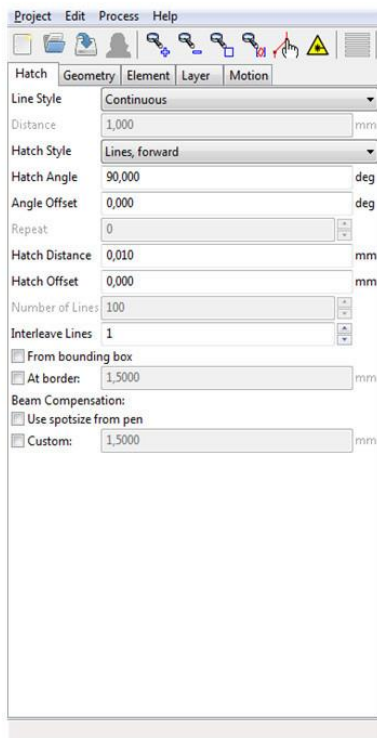
window shows state and power of laser. The detail of the printer process can also be set in the background program.



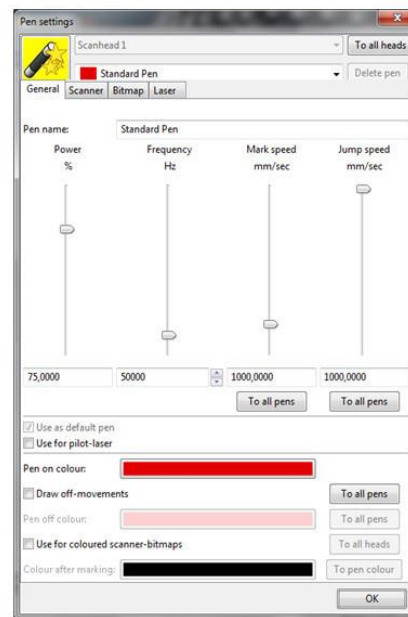
Figure 10 The software control panel of Microla printer.



(a)



(b)



(c)

Figure 11 (a)The interface of BeamConstruct, (b) Hatch settings, (c) Pen settings

Figure 11 shows the interface of BeamConstruct which is an integrated, stand-alone laser marking software solution for almost all kinds of laser scanner. In this work, we use it

as the laser control software. In the center of window (Figure 11 (a)), the geometry of the printed sample is shown which is one side of interdigitated electrode, the circle around the electrode is the shape of our platform (Figure 11 (b)) in the printer. When we import our STL file, the adjustment is needed to put our sample on center the platform. On the right side of the window, it shows each slice of our geometry and laser scanning process. At the left of window, it shows the settings of slices and hatch. In slice settings, we can set the thickness of layers also different laser scanning for each layer. Hatch settings can set the laser scan style. In this work, the laser scans in line and the distance between two scanning line is 0.01 mm. Also, the laser power, frequency, mark speed and jump speed can be set in Pen settings. Mark speed is a very important parameter also with laser power, these two can influence the polymerization of resin. In this work, we usually keep the mark speed at 1000 mm/s.

After the printing process is finished, an extra ultraviolet light treatment is need for electrodes to make sure the fully curing of resin. The extra curing process was done by Spot light source LC8 from Hamamatsu for 5 minutes at 100% power (4500 mW/cm^2).



Figure 12 Spot light source LC8 used in our work (right one with single lamp).

In this work, three thickness electrodes were printed, they are 0.5mm (5 layers), 1mm

(10 layers) and 2mm (20 layer). As often happens, the result of 3D printing can be slightly different from the desired one in terms of dimensions. Along Z axis, shrinkage or overcuring, due to difficulties in setting the right layer thickness, can lead to thinner or thicker parts. So, the final thickness of electrodes to test were 0.7mm, 1.1mm 1.3mm and 2.1mm. Another problem also shows up in our printing process, the size of electrodes will shrink after printing along XY plane. This problem can cause a miss-fit to the prepared substrates. So, enlarging the electrodes by 3.5%, the right dimensions were obtained

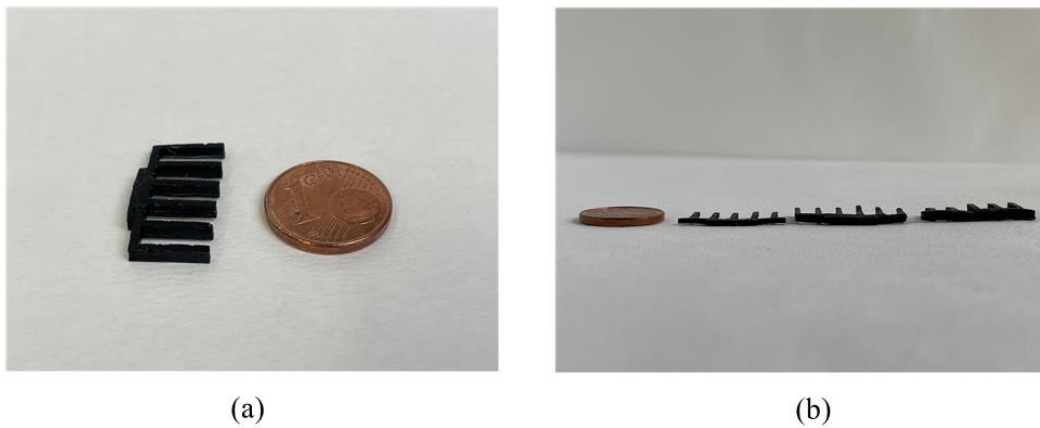


Figure 13 (a)Printed electrode and (b) electrodes in 0.7mm, 1.1mm, 2.1mm thickness.

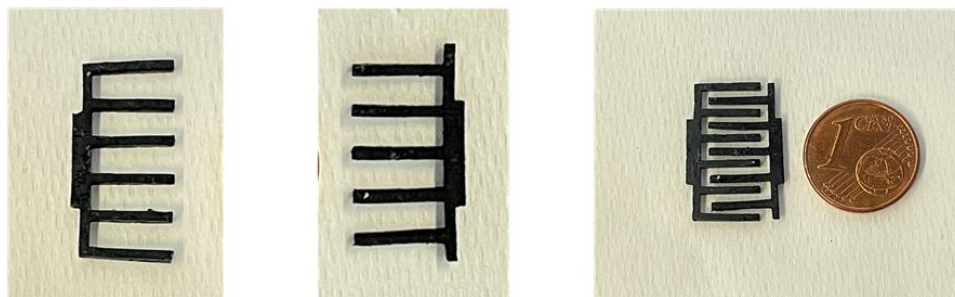


Figure 14 One couple of electrodes shows the deformation may cause a short circuit between two electrodes.

2.2.3 Assembly of supercapacitor

Three main parts of our supercapacitor are substrate, electrodes, chamber, and electrolyte.

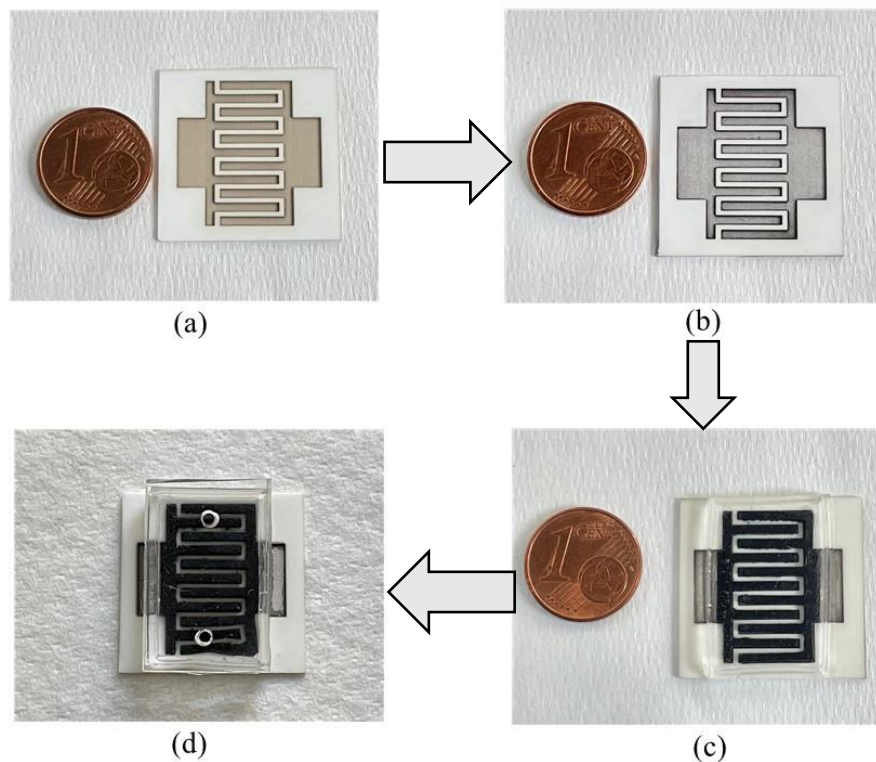


Figure 15 Assembly process of supercapacitor: (a) Etched alumina substrate; (b) Alumina substrate after sputter the platinum current collector; (c) inlay and glue electrodes and silicone chamber; (d) Enclosed cell with two holes for electrolyte injection.

Alumina was chosen for our substrate material because of its good smoothness, high thermal conductivity, superior mechanical strength, excellent resistance against chemical and high dielectric breakdown voltage. Because of its good smoothness, the platinum sputtering can be easily done. But as shown in Figure 13(b) and Figure 14, the

electrodes we printed have a deformation problem after taking them out of the printer. It is impossible to glue electrodes tightly with substrates to get a good contact with current collector. Also, we need avoid the possible contact between two electrodes. To solve the problems, the alumina substrates were etched by Microla Optoelectronics to get the same pattern as the hard mask (Figure 8(a)). The etching process was done by 70kHz, 50 W infrared pulsed laser at 1000 mm/s scan speed, and the etching depth is 200 μ m. An etched alumina substrate is shown in Figure 16.

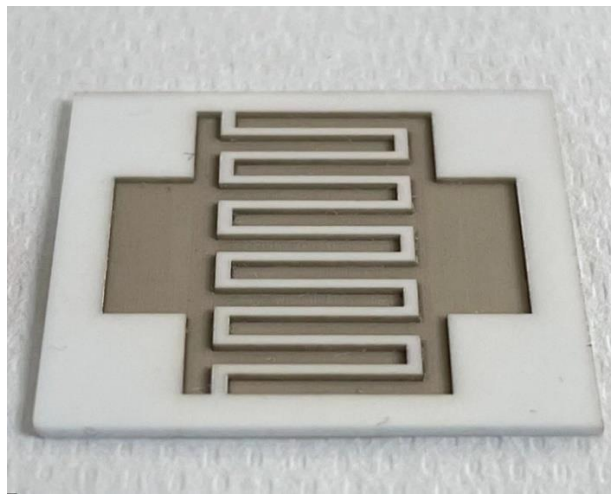


Figure 16 A close looking of etched alumina substrate.

Nest step, a platinum current collector is selectively deposited on the etched alumina substrates with the hard mask through sputtering process. The sputtering process was done by Q150T S sputter coater from Quorum Technologies. It is a gas flow sputtering (GFS) system working with argon gas and nitrogen gas. This technique is based on a hollow cathode effect, which transports the sputtered material to the substrate. Because the targets and substrates are facing each other, the hollow cathode effect results in a very high plasma density therefore it results in an efficient sputtering.[58] Because of unsmooth surface caused by etching process in the current collector area and the depth, we need a thicker platinum layer that means we need a longer sputtering process up to 200s. Alumina substrate with platinum current collector is shown in Figure 15(b) with a

silver color.

Then, electrodes can be assembled on the substrate. Electrodes are glued on the substrates by the resin which is as same as we used to print the electrodes. Firstly, the electrode bottom was gently dipped in the resin, make sure that such side of the electrode was covered by a thin layer of resin. Secondly, the electrode was inserted into the etched indentation and make a good contact with the platinum surface. Lastly, using the same UV light source (Figure 12), the resin was cured for a tight connection between electrodes and current collector.

The chamber walls were made by cured silicone in a polymethyl methacrylate (PMMA) mold. The PMMA mold is etched by laser maker. After silicone poured in the mold, cure it for 2 hours on an 80°C hot plate. Then the chamber wall can be glued on the substrate (Figure 15(c)). The top cover was also made by cured silicone. The cover was sealed on the wall later by silicone. The two holes on the cover is the window for electrolyte injection (Figure 15(d)).

Before injecting electrolyte, an annealing process was needed. The cells were heated up to 120°C in a vacuum oven and last for 1 hour then turn off the oven and wait for it cool down to room temperature. The annealing process can improve the electrical conductivity of electrodes and seal the chamber, as well as to post-cure the 3D printed object

In our experiment, a gel electrolyte was prepared. 6wt.% Polyvinyl alcohol (PVA) was solved in 88wt.% deionized water which are the ones giving the gel substance, and 6wt.% Potassium chloride (KCl) was solved in the gel substance which applies anions and cations. First, PVA need to be fully solved in deionized water by stirring and heated up 85°C. After KCl was solved, we got a transparent electrolyte in Figure 17.

After injecting electrolyte into the cell, another silicone cover was sealed to close the holes on chamber to prevent the water evaporation in long term measurement.

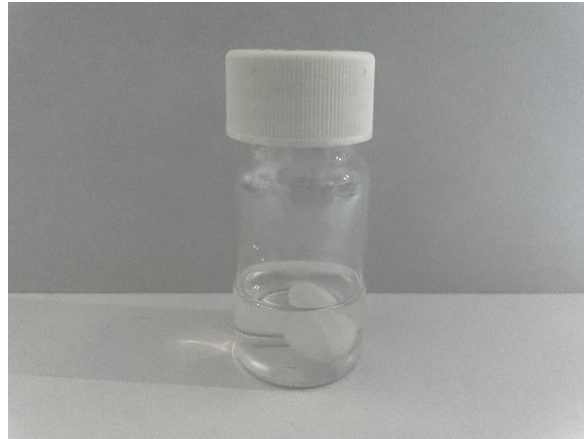


Figure 17 PVA/KCl electrolyte

2.2.4 Testing of supercapacitor

To evaluate supercapacitor performance, three basic parameters, cell capacitance, operating voltage, and equivalent series resistance are typically used to evaluate their energy and power performance. In research area, different materials, manufacturing processes, and cell designs bring additional factors can affect supercapacitor performance. In Figure 18, it is shown the possible factors can affect three essential parameters and test methods.

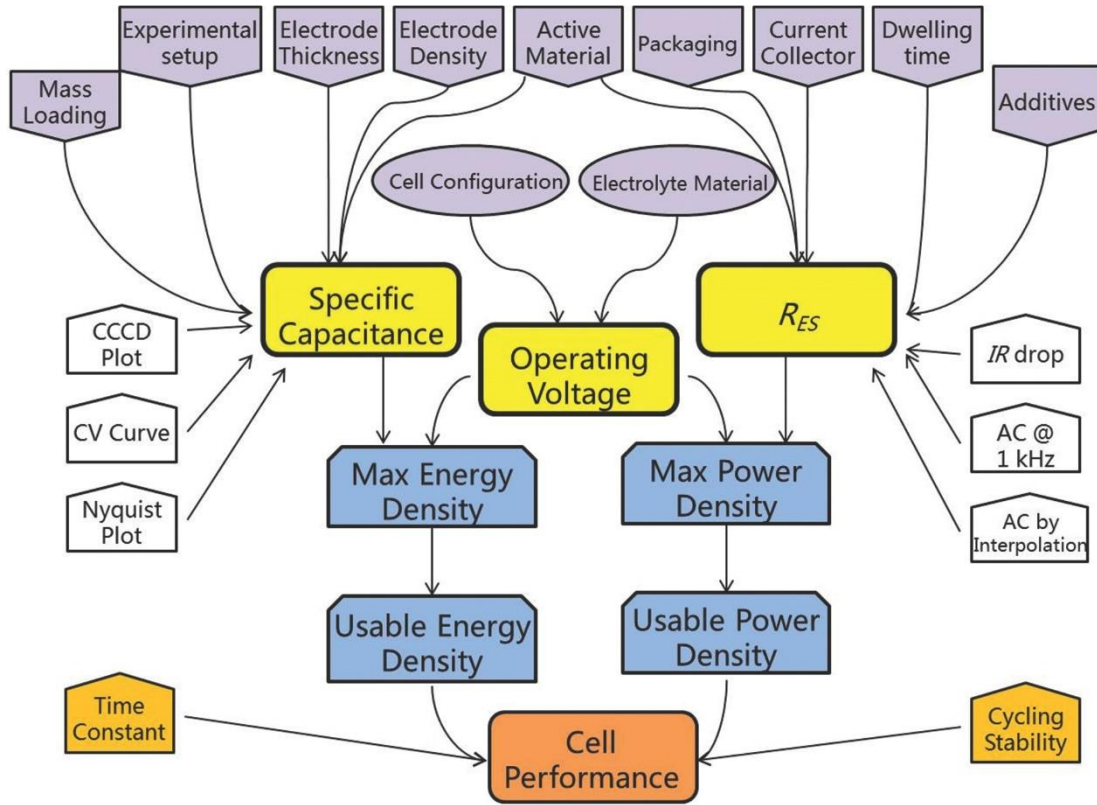


Figure 18 Key performance metrics, test methods and affecting factors for supercapacitors[59]

2.2.4.1 Characterization methods

There are three electrochemical characterization methods have been developed to characterize the performance of supercapacitors: Cyclic Voltammetry (CV), Constant Current Charge and Discharge (CCDC), and Electrochemical Impedance Spectroscopy (EIS).

In CV, a voltage signal sweep linearly within a potential window from V_{min} to V_{max} in a constant slope is applied between positive and negative electrodes for a two-electrode measurement. And the linear slope is called scan rate ν which usually measured in mV/s. When the voltage increases, the supercapacitor is charging, and the current is positive. When the voltage decreases, the supercapacitor is discharging, and the current is negative. The instantaneous current between two electrodes is measured.

The data are usually plotted $v(t)$ against $i(t)$. In a capacitor, current can be written in equation:

$$i(t) = C \frac{dv(t)}{dt} = Cv$$

where the $v(t)$ is the sweeping voltage, $i(t)$ is the instantaneous current, and C is the capacitance. In an ideal capacitor, the capacitance can keep constant, so the current can be kept constant and change direction with sweeping voltage, and the plot of CV shows a rectangle shape. But in a real case, by introducing the effect of resistive elements current will have a rising and dropping behavior. The shape of plot can also be affected by redox reactions from pseudo-supercapacitor materials. Redox peaks can be shown in the plot.

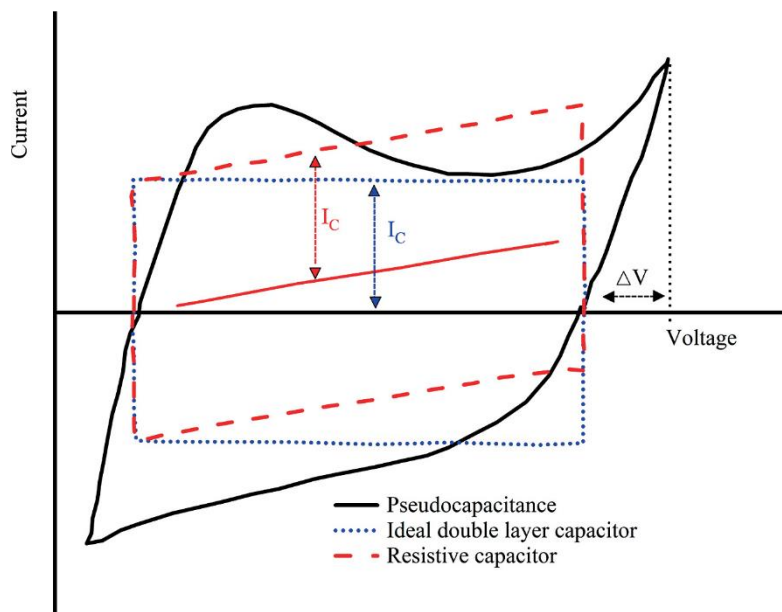


Figure 19 CV plot of ideal double layer capacitor, resistive capacitor and pseudocapacitor.[60]

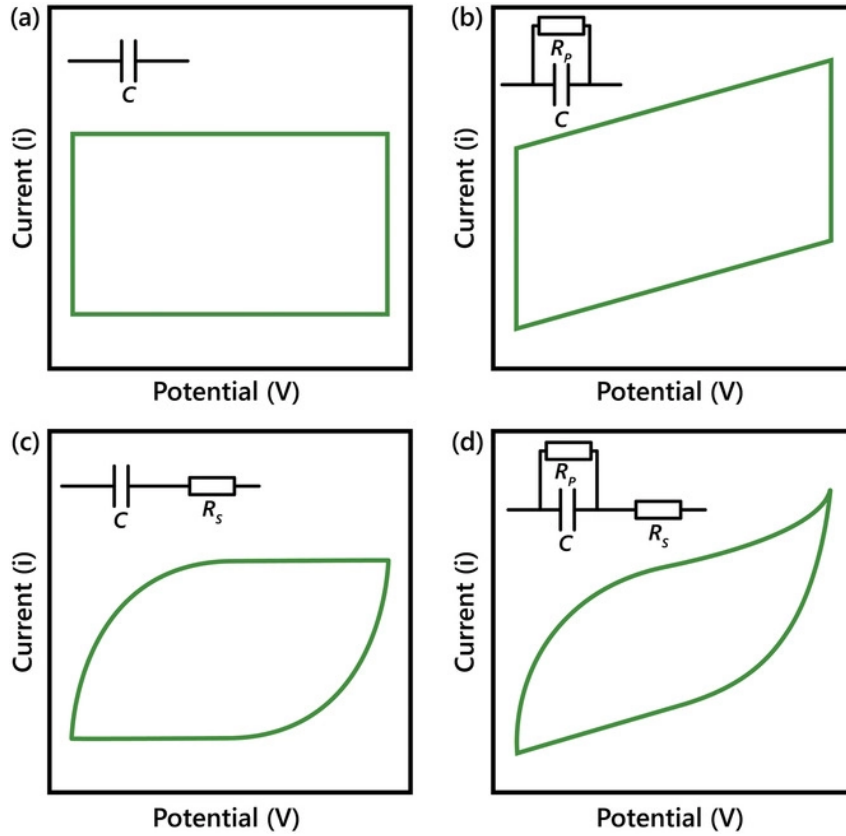


Figure 20 The equivalent circuit models introduced by Boonpakdee et al. to analysis the CV plot.[61]

In addition, the cell capacitance can be obtained from integration of the CV curves. The equations are following.

From the $i(t)$ - $v(t)$ curves:

$$C = \frac{1}{2v\Delta V} \int_{V_{min}}^{V_{max}} i(v)dv$$

From the $i(t)$ curves:

$$C = \frac{Q}{\Delta V} = \frac{1}{\Delta V} \int_0^t i(t)dt$$

In CV measurement, several scan rates can be set to investigate the supercapacitor performance. In general, the smaller scan rate is, the devices have more time to charge and discharge, more time to have redox reaction, and that will show us a larger

capacitance. In this work, 2, 5, 10, 20, 50, 100, 200 mV/s scan rates are used in our CV measurement and the potential window is 0 to 0.8V.

Constant Current Charge and Discharge (CCDC) as known as Charge Discharge Galvanostatic (CDG). CCCD test is the most widely used, most versatile and accurate method to characterize supercapacitor, and it also can be used it in cycling stability test. In CCDC measurement, a constant current is applied to the cell and the voltage is measured and limited in a voltage window. One cycle of measurement is that the cell is charged when the applied current is positive until the voltage reaches peak voltage, then the current switch its direction, and the cell start to discharge until the voltage reaches 0 V. This kind of cycles repeat in the CCDC test. The voltage under measured in a capacitor can be written in an equation:

$$v(t) = \frac{1}{C} \int_0^t i(t) dt = \frac{It}{C} = \frac{Q}{C}$$

where C is capacitance, Q is charge. In an ideal capacitor, the capacitance can keep constant during charge and discharge, so the plot of $v(t)$ is an isosceles triangle. If we introduce the resistance effect, the cures will show IR-drop.

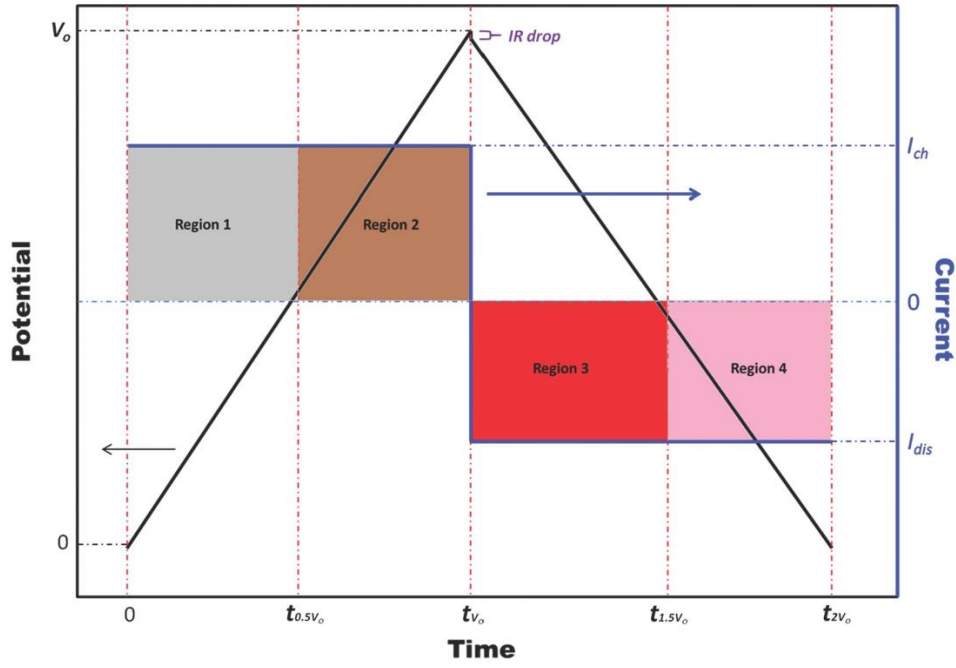


Figure 21 CCCD curve of a supercapacitor.[59]

From the results of CCCD, the capacitance can be easily calculated by:

$$C = \frac{Q}{\Delta V} = \frac{1}{\Delta V} \int_0^t i(t) dt = \frac{It}{\Delta V}$$

where t is the time of charge or discharge corresponding to the potential change ΔV .

For more accurate result, the IR drop need to be considered and adjust in the calculation.

And the discharge curve is often used.

$$C = \frac{I_{dis} t_{V_0-2V_0}}{V_0 - V_{IR-drop}}$$

In our work, all the results were got from CCCD test. The Capacitance C was calculated by Energy E and Charge Q :

$$E = \int v(t) i(t) dt$$

$$Q = \int i(t) dt$$

$$C = \frac{Q^2}{2E}$$

Also, coulombic efficiency is an important quantifiable indicator for the reversibility of supercapacitor, and it shows the internal electric quantity dissipation in the charge-discharge process. The coulombic efficiency coefficient is η :

$$\eta = \frac{Q_{discharge}}{Q_{charge}}$$

where Q_{charge} is the charge quantity during the devices charging time, and $Q_{discharge}$ is the charge quantity during the discharge time. The coulombic efficiency of electrochemical energy storage devices is expected to be 1.

EIS test performs impedance measurements by applying a sinus voltage signal to measure the impedance of the cell as a function of frequency. For every frequency within the frequency range, the responded current is measured. The result data are usually plotted in Bode plot and Nyquist plot. Bode plot show a frequency response of the devices and is usually included a Bode magnitude which expresses the magnitude(dB) of frequency response and a Bode phase plot which expresses the phase shift against frequency. Nyquist plot shows a frequency response of impedance. It represents negative imaginary parts impedance versus the real parts of the complex impedance of electrochemical devices. A Nyquist plot curve can also show a capacitor behavior if the curve goes up vertically. Furthermore, two EIS test can be performed before and after a cycling stability test and the shift of two Nyquist plot can also show the stability of devices.

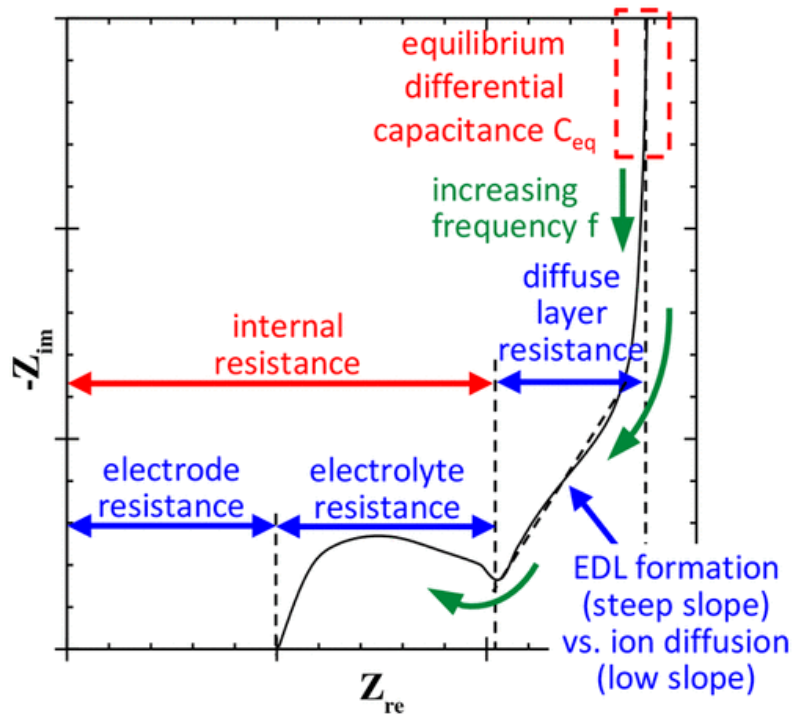


Figure 22 A general Nyquist plot for an electrical double layer capacitor.[62]

2.2.4.2 Instruments

In our measurement, two instruments were used, VMP3 from BioLogic and ARBIN BT2000.

VMP3 is a research grade workstation has maximum 16 independent potentiostat channels. Each installed potentiostat can be connected to a high current booster channel. It can be used in electroanalytical, general electrochemistry, energy storage, and batteries applications. With the powerful and intuitive advanced software EC-Lab which can perform electrochemistry measurements, we performed CV, CCCD, and EIS tests in VMP3

ARBIN BT2000 is a battery test equipment which also have multiple independent channels. It is controlled by an external PC with MITs Pro software. In BT2000, we performed the cycling stability test by using CCCD technique.

2.2.4.3 Cell connection

Usually, two different methods can be performed to supercapacitor test: three-electrode measurement and two-electrode measurement.

In three-electrode measurement, three electrodes are involved, working electrode (WE) which is the main electrode under test, counter electrode (CE) who acts the other half of the cell, and reference electrode (REF) who acts as a reference in measuring and controlling the WE. The controlled voltage is always the one between WE and REF, and the current always flow between WE and CE. Ideally, there is no current flows in the REF branch, only voltage drop on REF.

In two-electrode measurement, only WE and CE are involved. The potential is applied between the WE and CE, and the resulting current is under measured. Two-electrode measurement can be easily transferred from three-electrode measurement by connecting REF and CE together as a counter electrode.

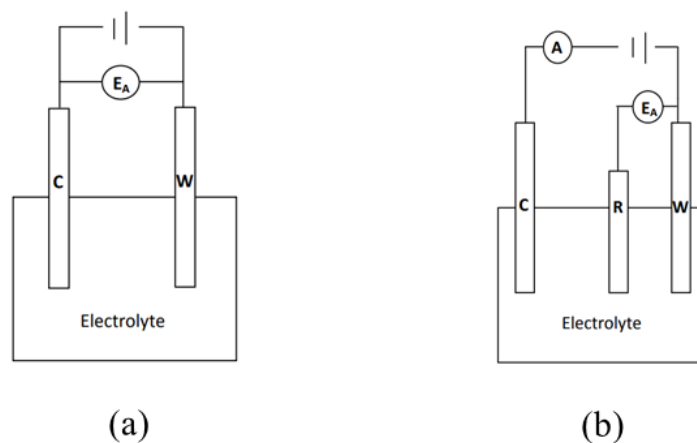
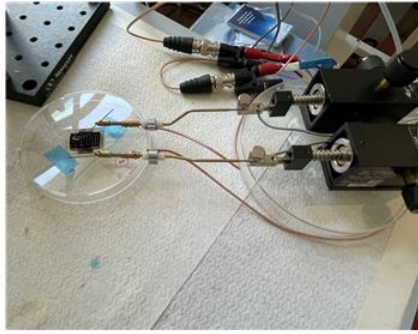
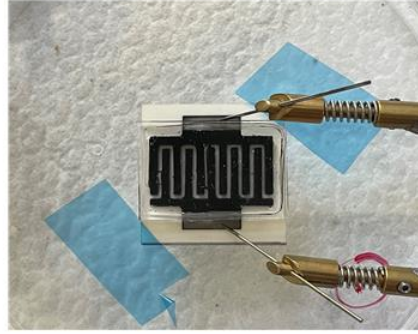


Figure 23 (a) two-electrode system; (b) three-electrode system

In our work, we used two-electrode measurement. The cables from instruments were connected to two micromanipulators. By Operating the micromanipulators, we touched two probes to the platinum current collectors.



(a)



(b)

Figure 24 (a) a cell is connected to the instrument by two micromanipulators; (b) a close looking of the probes are touched to the platinum current collector.

3 Results and Discussion

3.1 Results data analysis

Several issues were solved in order to test the devices, such as bad connection between electrodes and current collector led by deformation of electrodes, unwanted short connection between electrodes also because of the deformation of electrodes, electrodes shrinking problem after printing. After optimizing the design and fabrication of our supercapacitor, we tried to print 5 layers, 10 layers, 20 layers electrodes which should be 0.5mm, 1.0mm, and 2mm. Because of the problem of our 3D printer, we didn't get an accuracy 0.1mm per layer. At the end, we measured the real thickness of printed electrodes, we got 0.7mm, 1.1mm, 1.3mm, and 2.1 mm electrodes. For every thickness, we fabricated and tested three devices and the results are shown in following.

3.1.1 0.7mm thickness electrode device

In Table 1, it is shown the capacitance we measured from 0.7mm thickness electrode devices, and all the results retrieved from Constant Current Charge and Discharge (CCCD) measurement. The maximum capacitance we got is 31.98mF, specific capacitance 10.95mF/cm² and 15.65 mF/cm³ at 5μA/cm² current density.

	Capacitance [mF]	Areal capacitance [mF/cm ²]	Volumetric capacitance [mF/cm ³]
sample1	30.75	10.53	15.04
sample2	29.56	10.12	14.46
sample3	31.98	10.95	15.65

Table 1 Capacitance and specific capacitance of 0.7mm thickness devices in CCCD measurement at 5 μ A/cm² current density.

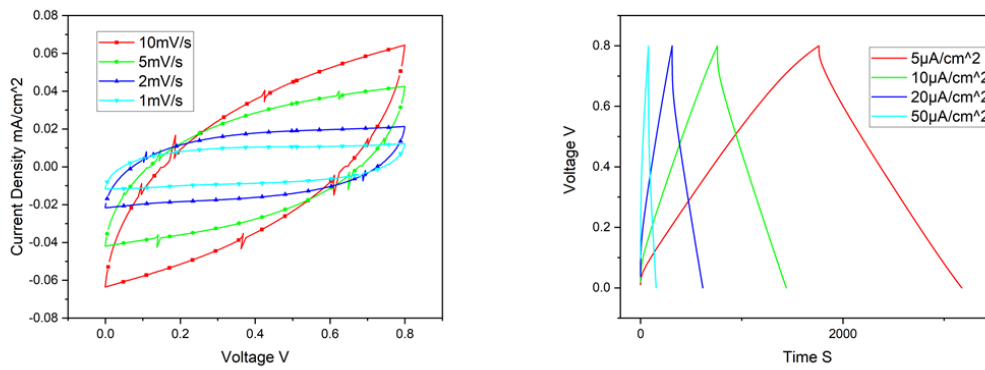


Figure 25 CV plot (left) at 1mV/s, 2mV/s, 5mV/s, and 10mV/s scan rates, and CCCD plot (right) at $5\mu\text{A}/\text{cm}^2$, $10\mu\text{A}/\text{cm}^2$, $20\mu\text{A}/\text{cm}^2$, $50\mu\text{A}/\text{cm}^2$ of 0.7mm thickness device.

In Figure 25, it is shown the CV and CCCD test result. In CV plot, when the scan rate is 1mV/s which is the slowest one, the curve shows a very standard capacitor behavior with the effect of series resistance, the general shape is a rectangle with a smooth angle at up left and down right. When the scan rate increased, the shape of CV plot turns into a leaf-shape like curves because of the effect of parallel resistance in the devices. Also because of diffusion problem, and electrodes and device are globally resistive, it shows a low value of capacitance. In CCCD plot, it is shown the charge discharge behavior with an IR-drop. At low current density $5\mu\text{A}/\text{cm}^2$, it took the longest time to charge and discharge, and it provided the largest value of capacitance. By looking the charge and discharge time, we can say the device has a good coulombic efficiency.

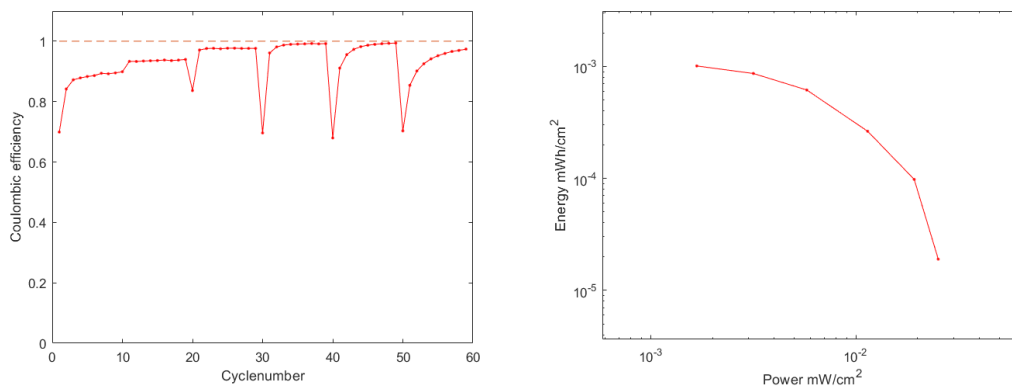


Figure 26 0.7mm thickness device Coulombic efficiency (left) and Ragone plot (right) at 5, 10, 2,

50,100, and 200 $\mu\text{A}/\text{cm}^2$

In Figure 26, it is shown the coulombic efficiency of 0.7mm device 10 cycles per current density and Ragone plot whose energy and power are from the last cycle at each current density in CCCD test. The coulombic efficiency of our devices is very high and close to one in higher current density after few cycles of working and it show very good capacitor behavior. Ragone plot is a curve plotted by energy versus power. It can show the performance of electrochemical energy storage devices. It intuitively shows the relationship between the energy and power of the devices and how the devices match the comparable and competitive systems. Also, Ragone plot can always show which performance region the device is. Our 0.7mm device is on the region of energy density 10^{-5} to 10^{-3} mWh/cm² and power density 10^{-3} mW/cm² to 10^{-1} mW/cm². If we match our Ragone plot in Figure 27, it shows that the 0.7mm devices can be used for sensors (temperature, pressure, humidity, optic, acoustic, etc.).

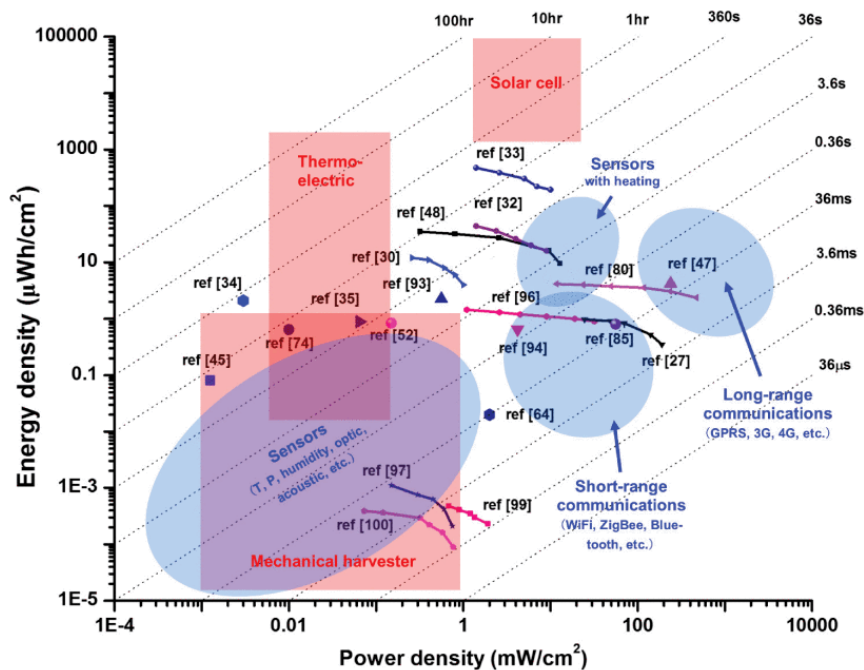


Figure 27 Area-normalized Ragone plots of representative supercapacitor and performance requirement to work in different applications such as energy harvesters, sensors, and wireless communications.[63]

3.1.2 1.1mm thickness electrode cell

In Table 2, it is shown the capacitance we measured from 0.7mm thickness electrode devices, and all the results were gotten from Constant Current Charge and Discharge (CCCD) measurement. The maximum capacitance we got is 36.42mF, specific capacitance 12.47mF/cm² and 11.34mF/cm³ at 5μA/cm² current density. The capacitance result we got from 1.1mm devices are little higher than 0.7mm devices. But if we compare the specific capacitance in volume, the increase of capacitance is not respect to the increase of thickness.

	Capacitance [mF]	Areal capacitance [mF/cm ²]	Volumetric capacitance [mF/cm ³]
sample1	31.08	10.64	9.68
sample2	30.97	10.61	9.64
sample3	36.42	12.47	11.34

Table 2 Capacitance and specific capacitance of 1.1mm thickness devices in CCCD measurement at 5 μ A/cm² current density.

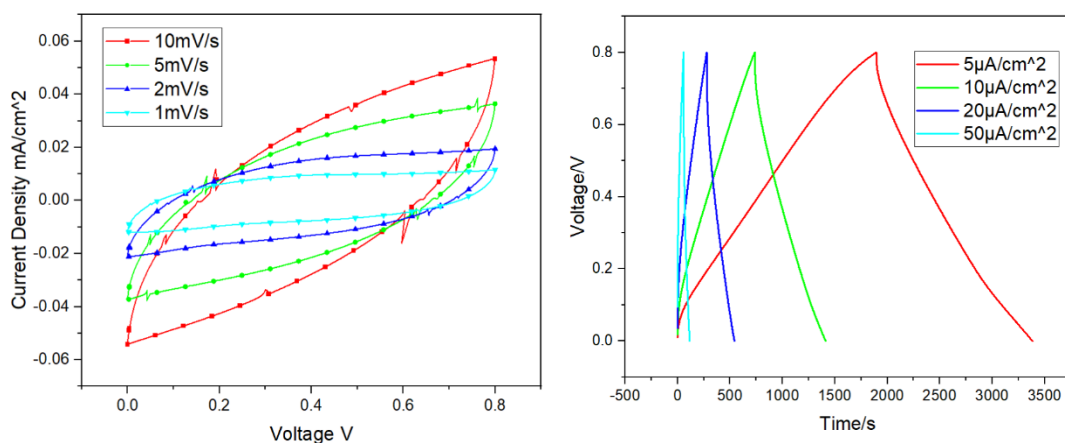


Figure 28 CV plot (left) at 1mV/s, 2mV/s, 5mV/s, and 10mV/s scan rates, and CCCD plot (right) at 5μA/cm², 10μA/cm², 20μA/cm², 50μA/cm² of 1.1mm thickness device.

In Figure 28, it is shown the CV plot and CCCD plot, there is no big different from 0.7mm devices. In Figure 29, it also shows high coulombic efficiency and the Ragone plot presents at the same region as 0.7mm devices.

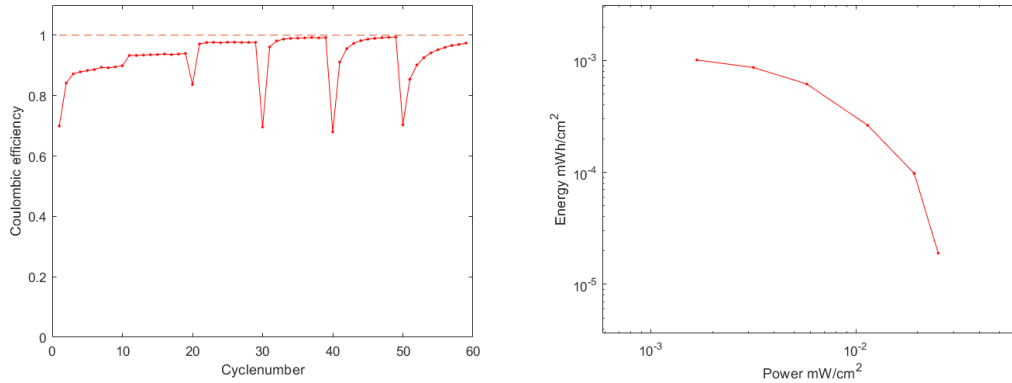


Figure 29 1.1mm thickness device Coulombic efficiency (left) and Ragone plot (right) at 5, 10, 2, 50,100, and 200 μ A/cm²

3.1.3 1.3mm thickness electrode cell

In Table 3, it is shown the capacitance we measured from 0.7mm thickness electrode devices, and all the results were gotten from Constant Current Charge and Discharge (CCCD) measurement. The maximum capacitance we got is 34.22mF, specific capacitance 11.72mF/cm² and 9.01mF/cm³ at 5 μ A/cm² current density. Compare with 1.1mm and 1.3mm devices, we can see a clear increase of device capacitance. But the volumetric capacitance is lower than previous two thickness devices

	Capacitance [mF]	Areal capacitance [mF/cm ²]	Volumetric capacitance [mF/cm ³]
sample1	33.12	11.34	8.72
sample2	33.23	11.38	8.75
sample3	34.22	11.72	9.01

Table 3 Capacitance and specific capacitance of 1.3mm thickness devices in CCCD measurement at 5 μ A/cm² current density.

In Figure 30, it is shown the CV plot and CCCD plot, there is no big different from previous shown devices. In Figure 31, it also shows high coulombic efficiency and the Ragone plot presents at the same region as 0.7mm and 1.1mm devices.

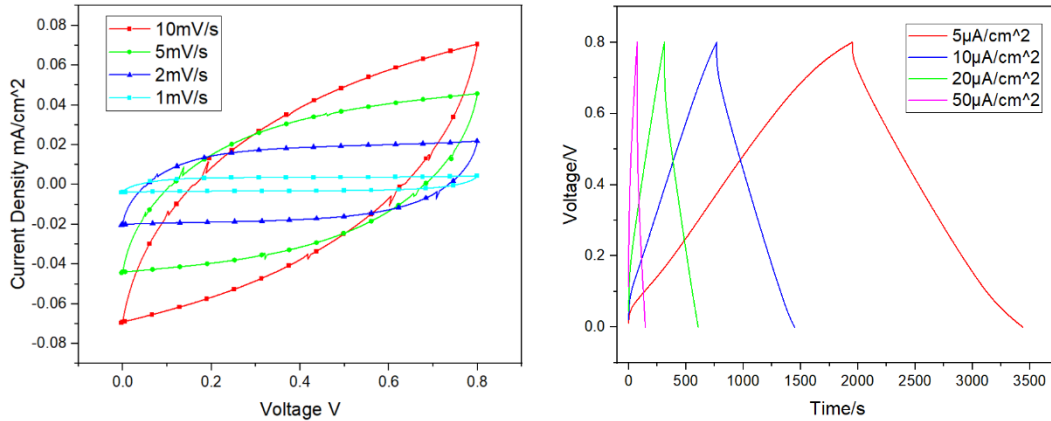


Figure 30 CV plot (left) at 1mV/s, 2mV/s, 5mV/s, and 10mV/s scan rates, and CCCD plot (right) at $5\mu\text{A}/\text{cm}^2$, $10\mu\text{A}/\text{cm}^2$, $20\mu\text{A}/\text{cm}^2$, $50\mu\text{A}/\text{cm}^2$ of 1.3mm thickness device.

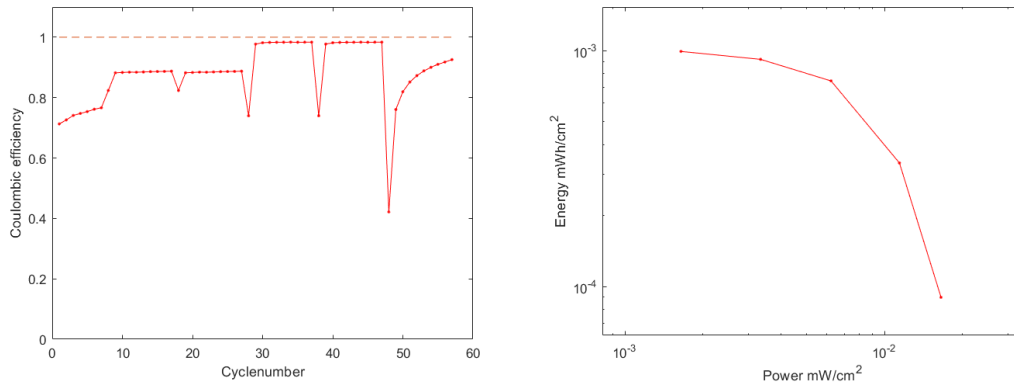


Figure 31 1.3mm thickness device Coulombic efficiency (left) and Ragone plot (right) at 5, 10, 2, 50, 100, and $200\mu\text{A}/\text{cm}^2$

3.1.4 2.1mm thickness electrode cell

In Table 4, it is shown the capacitance we measured from 0.7mm thickness electrode devices, and all the results were gotten from Constant Current Charge and Discharge (CCCD) measurement. The maximum capacitance we got is 56.80mF, specific

capacitance 11.72mF/cm² and 9.01mF/cm³ at 5μA/cm² current density. In thickest devices we got the maximum capacitance of all tested devices.

	Capacitance [mF]	Areal capacitance [mF/cm ²]	Volumetric capacitance [mF/cm ³]
sample1	42.30	14.49	6.90
sample2	56.80	19.45	9.26
sample3	25.51	8.74	4.16

Table 4 Capacitance and specific capacitance of 2.1mm thickness devices in CCCD measurement at 5 μ A/cm² current density.

In Figure 32, it is shown the CV plot and CCCD plot, there is no big different from 0.7mm devices. In Figure 33, it also shows high coulombic efficiency and the Ragone plot presents at the same region as 0.7mm devices.

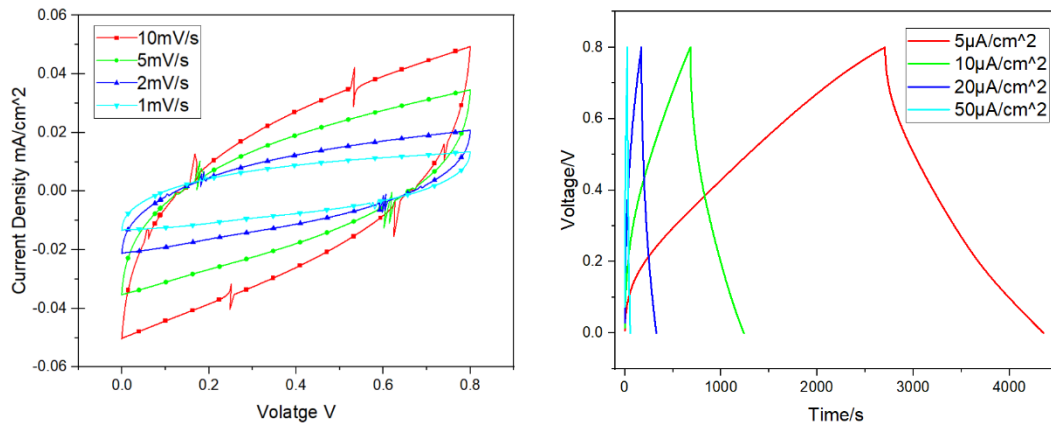


Figure 32 CV plot (left) at 1mV/s, 2mV/s, 5mV/s, and 10mV/s scan rates, and CCCD plot (right) at 5μA/cm², 10μA/cm², 20μA/cm², 50μA/cm² of 2.1mm thickness device.

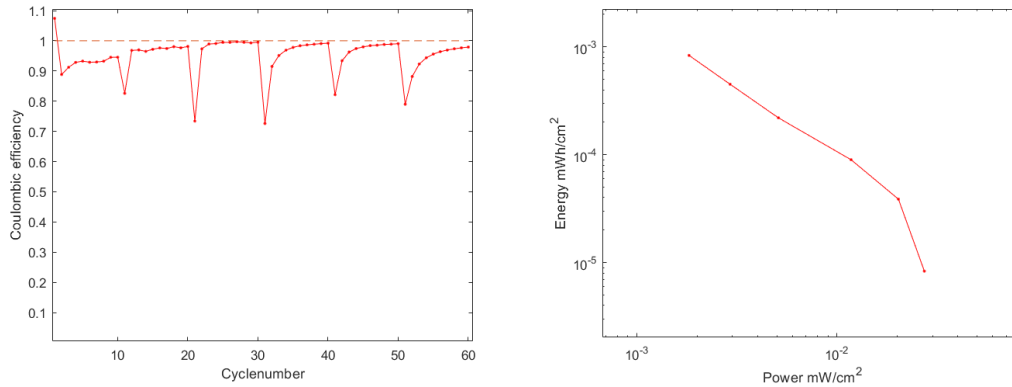


Figure 33 2.1mm thickness device Coulombic efficiency (left) and Ragone plot (right) at 5, 10, 2, 50,100, and 200 μ A/cm²

3.1.5 Comparison

In Table 5, it is shown the maximum capacitance from 4 different thickness devices. We can clearly see the capacitance is not increase linearly by the thickness increase. And the volumetric capacitance of 2.1mm device is much lower than 0.7mm devices. The 2.1mm electrodes were printed by 18 layers, and 0.7mm electrodes were printed by 5 layer, so there is higher contact resistance between adjacent layers and reduce the electronic transmission efficiency in 2.1mm devices.[64]

	Capacitance [mF]	Areal capacitance [mF/cm ²]	Volumetric capacitance [mF/cm ³]
0.7mm	31.98	10.95	15.65
1.1mm	36.42	12.47	11.34
1.3mm	34.22	11.72	9.01
2.1mm	56.80	19.45	9.26

Table 5 Capacitance and specific capacitance of maximum values from 4 different thickness devices.

In Figure 34(a), it is shown the CV plot of 0.7mm, 1.1mm, 1.3mm, 2.1mm thickness devices in one graph at 1mV/s scan rate. In this graph, we can see the 1.3mm device

shows the best widely open curve and more close to a rectangular shape. If we check the result in Table 3, it shows a very close result of three samples. We can say the group of 1.3mm device was the best devices from fabrication domain. We can also see the CV curve of 2.1mm devices is the worst because of the resistance element. In Figure 34(b), it is shown the CCCD plot of 4 different thickness devices. The curves of 0.7mm, 1.1mm and 1.3mm devices are very close because they get close capacitance and IR-drop. The curves of 2.1mm is different, it has much longer cycle time at the same current density because of much larger capacitance. In Figure 34(c), it shows the Ragone plot of 4 thickness devices. The curves are very close. It shows a very close performance of all of thickness. They are all at the same performance region for sensors application.

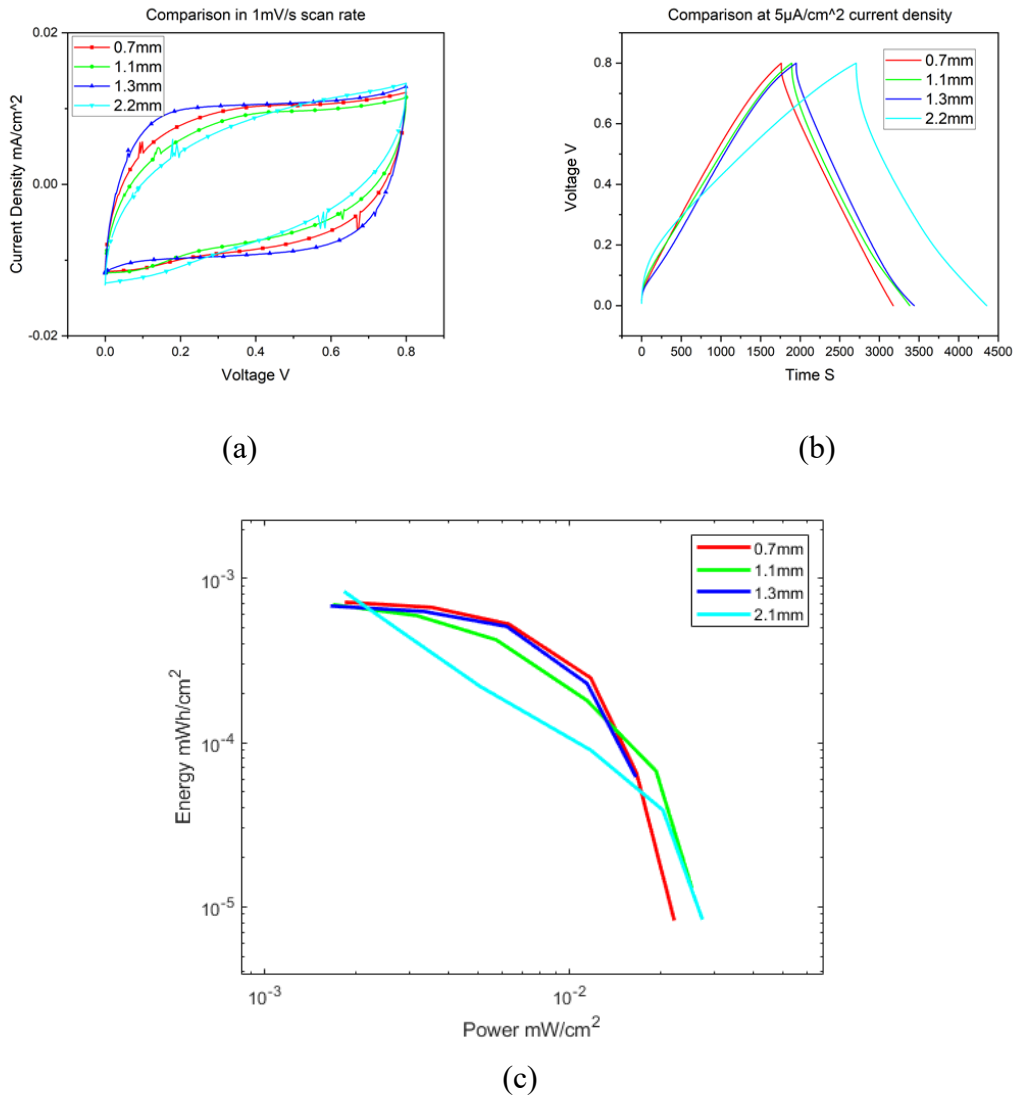


Figure 34 (a) CV plot of 4 different thickness devices at 1mV/s scan rate; (b) CCCD plot of 4

different thickness devices at $5 \mu \text{A}/\text{cm}^2$; (c) Ragone plot of 4 different thickness devices.

3.1.6 Cycling stability

The cycling stability was tested in CCCD measurement at $10 \mu\text{A}/\text{cm}^2$ current density. The cycling number was up to 500 and it took 2 weeks (14 days) to finish the cycling stability test. The results of the test is shown in Figure 35, capacity retention and coulombic efficiency. We can see the capacitance was smaller than the maximum value at the beginning, it increased and reached the maximum capacitance after around 20 cycles, then it decreased very slowly. After running 500 cycles, 14 days, the capacity retention remained 92%. The coulombic efficiency reached a high value after several cycles then increased very slowly from 94% to 97%, after 500 cycles the coulombic efficiency was 96.7%. It shows the 3D printed PEDOT:PEDGA resin is very a stable material for supercapacitor application. We didn't carry on the stability test for more cycles, because of the electrolyte evaporation issue.

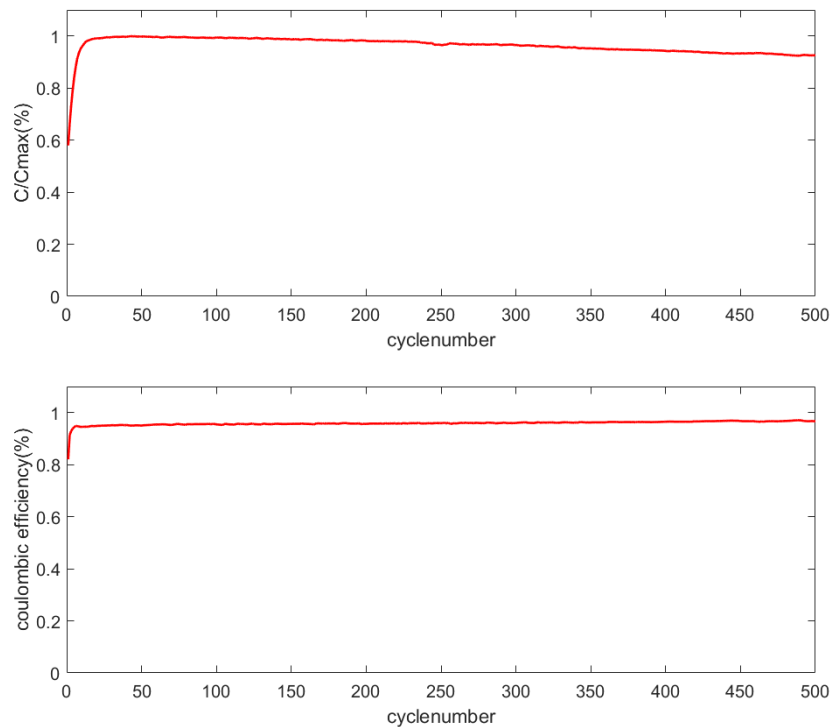


Figure 35 Capacity retention and Coulombic efficiency in cycling stability test.

3.2 Conclusion

In conclusion, our 3D printable electrically conductive PEDOT:PEGDA resin can find application in the energy storage field, and the supercapacitor manufactured by this resin can achieve maximum capacitance of 19.45 mF/cm^2 in our experiment. According to the performance of energy and power density, our supercapacitor can be used in sensor applications. Additionally, the capacity retention of our supercapacitor remained 92% and coulombic efficiency was up to 96.7% after 500 cycles (14 days) in the cycling stability test.

The PEDOT:PEGDA resin shows a good performance applied in energy storage application. The stability of this material also be verified from the cycling stability test. The electrodes remain almost the same capacity after weeks charge discharge test, and the electrodes can keep a strong structure from the gel electrolyte.

4 References

- [1] M. Kamran and A. Saxena, “A Comprehensive Study on 3D Printing Technology,” 2016.
- [2] T. Rayna and L. Striukova, “From rapid prototyping to home fabrication: How 3D printing is changing business model innovation,” *Technological Forecasting and Social Change*, vol. 102, pp. 214–224, Jan. 2016, doi: 10.1016/j.techfore.2015.07.023.
- [3] Z. Li, Z. Wang, X. Gan, D. Fu, G. Fei, and H. Xia, “Selective Laser Sintering 3D Printing: A Way to Construct 3D Electrically Conductive Segregated Network in Polymer Matrix,” *Macromolecular Materials and Engineering*, vol. 302, no. 11, Nov. 2017, doi: 10.1002/mame.201700211.
- [4] F. Fina, A. Goyanes, S. Gaisford, and A. W. Basit, “Selective laser sintering (SLS) 3D printing of medicines,” *International Journal of Pharmaceutics*, vol. 529, no. 1–2, pp. 285–293, Aug. 2017, doi: 10.1016/j.ijpharm.2017.06.082.
- [5] C. Gosselin *et al.*, “Large-scale 3D printing of ultra-high performance concrete-a new processing route for architects and builders”, doi: 10.1016/j.matdes.2016.03.097i.
- [6] S. H. Huang, P. Liu, A. Mokasdar, and L. Hou, “Additive manufacturing and its societal impact: A literature review,” *International Journal of Advanced Manufacturing Technology*, vol. 67, no. 5–8. pp. 1191–1203, Jul. 2013. doi: 10.1007/s00170-012-4558-5.
- [7] J. Huang, Q. Qin, and J. Wang, “A review of stereolithography: Processes and systems,” *Processes*, vol. 8, no. 9. MDPI AG, Sep. 01, 2020. doi: 10.3390/PR8091138.
- [8] S. C. Ligon, R. Liska, J. Stampfl, M. Gurr, and R. Mülhaupt, “Polymers for 3D Printing and Customized Additive Manufacturing,” *Chemical*

Reviews, vol. 117, no. 15. American Chemical Society, pp. 10212–10290, Aug. 09, 2017. doi: 10.1021/acs.chemrev.7b00074.

- [9] U. Kalsoom, P. N. Nesterenko, and B. Paull, “Recent developments in 3D printable composite materials,” *RSC Advances*, vol. 6, no. 65. 2016. doi: 10.1039/c6ra11334f.
- [10] S. J. Leigh, C. P. Purssell, J. Bowen, D. A. Hutchins, J. A. Covington, and D. R. Billson, “A miniature flow sensor fabricated by micro-stereolithography employing a magnetite/acrylic nanocomposite resin,” *Sensors and Actuators, A: Physical*, vol. 168, no. 1, 2011, doi: 10.1016/j.sna.2011.03.058.
- [11] S. A. Skoog, P. L. Goering, and R. J. Narayan, “Stereolithography in tissue engineering,” *Journal of Materials Science: Materials in Medicine*, vol. 25, no. 3. 2014. doi: 10.1007/s10856-013-5107-y.
- [12] A. K. Au, W. Lee, and A. Folch, “Mail-order microfluidics: Evaluation of stereolithography for the production of microfluidic devices,” *Lab on a Chip*, vol. 14, no. 7, 2014, doi: 10.1039/c3lc51360b.
- [13] J. Xue *et al.*, “Stereolithographic 3D Printing-Based Hierarchically Cellular Lattices for High-Performance Quasi-Solid Supercapacitor,” *Nano-Micro Letters*, vol. 11, no. 1, 2019, doi: 10.1007/s40820-019-0280-2.
- [14] A. Khan *et al.*, “Low-cost carbon fillers to improve mechanical properties and conductivity of epoxy composites,” *Polymers (Basel)*, vol. 9, no. 12, 2017, doi: 10.3390/polym9120642.
- [15] V. Strongone, M. Bartoli, P. Jagdale, R. Arrigo, A. Tagliaferro, and G. Malucelli, “Preparation and characterization of UV-LED curable acrylic films containing biochar and/or multiwalled carbon nanotubes: Effect of the filler loading on the rheological, thermal and optical properties,” *Polymers (Basel)*, vol. 12, no. 4, 2020, doi: 10.3390/polym12040796.

- [16] C. W. Foster *et al.*, “3D Printed Graphene Based Energy Storage Devices,” *Scientific Reports*, vol. 7, 2017, doi: 10.1038/srep42233.
- [17] T. S. Hansen, K. West, O. Hassager, and N. B. Larsen, “Highly stretchable and conductive polymer material made from poly(3,4-ethylenedioxythiophene) and polyurethane elastomers,” *Advanced Functional Materials*, vol. 17, no. 16, 2007, doi: 10.1002/adfm.200601243.
- [18] K. Sun *et al.*, “Review on application of PEDOTs and PEDOT:PSS in energy conversion and storage devices,” *Journal of Materials Science: Materials in Electronics*, vol. 26, no. 7. Springer New York LLC, pp. 4438–4462, Jul. 24, 2015. doi: 10.1007/s10854-015-2895-5.
- [19] D. Villers *et al.*, “The Influence of the Range of Electroactivity and Capacitance of Conducting Polymers on the Performance of Carbon Conducting Polymer Hybrid Supercapacitor,” *Journal of The Electrochemical Society*, vol. 150, no. 6, 2003, doi: 10.1149/1.1571530.
- [20] B. Anothumakkool *et al.*, “Pt- and TCO-Free Flexible Cathode for DSSC from Highly Conducting and Flexible PEDOT Paper Prepared via in Situ Interfacial Polymerization,” *ACS Applied Materials and Interfaces*, vol. 8, no. 1, 2016, doi: 10.1021/acsami.5b09579.
- [21] J. Yang *et al.*, “A robust inter-connecting layer for achieving high performance tandem polymer solar cells,” *Advanced Materials*, vol. 23, no. 30. 2011. doi: 10.1002/adma.201100221.
- [22] G. Scordo *et al.*, “A novel highly electrically conductive composite resin for stereolithography,” *Materials Today Communications*, vol. 19, pp. 12–17, Jun. 2019, doi: 10.1016/j.mtcomm.2018.12.017.
- [23] M. Winter and R. J. Brodd, “What are batteries, fuel cells, and supercapacitors?,” *Chemical Reviews*, vol. 104, no. 10, pp. 4245–4269, Oct. 2004, doi: 10.1021/cr020730k.

- [24] G. L. Bullard, H. B. Sierra-Alcazar, H. L. Lee, and J. L. Morris, "Operating principles of the ultracapacitor," *IEEE Transactions on Magnetics*, vol. 25, no. 1, pp. 102–106, 1989, doi: 10.1109/20.22515.
- [25] L. G. González, R. Chacon, B. Delgado, D. Benavides, and J. Espinoza, "Study of Energy Compensation Techniques in Photovoltaic Solar Systems with the Use of Supercapacitors in Low-Voltage Networks," *Energies (Basel)*, vol. 13, no. 15, 2020, doi: 10.3390/en13153755.
- [26] I. Hussain Panhwar *et al.*, "Mitigating power fluctuations for energy storage in wind energy conversion system using supercapacitors," *IEEE Access*, vol. 8, 2020, doi: 10.1109/ACCESS.2020.3031446.
- [27] I. Azizi and H. Radjeai, "A new strategy for battery and supercapacitor energy management for an urban electric vehicle," *Electrical Engineering*, vol. 100, no. 2, 2018, doi: 10.1007/s00202-017-0535-1.
- [28] J. P. Kruth, M. C. Leu, and T. Nakagawa, "Progress in additive manufacturing and rapid prototyping," *CIRP Annals - Manufacturing Technology*, vol. 47, no. 2, 1998, doi: 10.1016/S0007-8506(07)63240-5.
- [29] W. K. Swainson, "METHOD, MEDIUM AND APPARATUS FOR PRODUCING THREE-DIMENSIONAL FIGURE PRODUCT," 1971.
- [30] E. Richard *et al.*, "Apparatus for production of three-dimensional objects by stereolithography," *US Patent 4,575,330*, vol. 2, no. 12, 2011.
- [31] M. Hegde *et al.*, "3D Printing All-Aromatic Polyimides using Mask-Projection Stereolithography: Processing the Nonprocessable," *Advanced Materials*, vol. 29, no. 31, 2017, doi: 10.1002/adma.201701240.
- [32] J. R. Tumbleston *et al.*, "Continuous liquid interface production of 3D objects," *Science (1979)*, vol. 347, no. 6228, 2015, doi: 10.1126/science.aaa2397.
- [33] M. Shusteff *et al.*, "One-step volumetric additive manufacturing of complex polymer structures," *Science Advances*, vol. 3, no. 12, 2017, doi:

10.1126/sciadv.aao5496.

- [34] Y. G. Im, S. I. Chung, J. H. Son, Y. D. Jung, J. G. Jo, and H. D. Jeong, “Functional prototype development: Inner visible multi-color prototype fabrication process using stereo lithography,” in *Journal of Materials Processing Technology*, 2002, vol. 130–131. doi: 10.1016/S0924-0136(02)00826-9.
- [35] J. W. Choi, H. C. Kim, and R. Wicker, “Multi-material stereolithography,” *Journal of Materials Processing Technology*, vol. 211, no. 3, 2011, doi: 10.1016/j.jmatprotec.2010.10.003.
- [36] K. v. Wong and A. Hernandez, “A Review of Additive Manufacturing,” *ISRN Mechanical Engineering*, vol. 2012, pp. 1–10, Aug. 2012, doi: 10.5402/2012/208760.
- [37] S. Saleh Alghamdi, S. John, N. Roy Choudhury, and N. K. Dutta, “polymers Additive Manufacturing of Polymer Materials: Progress, Promise and Challenges,” 2021, doi: 10.3390/polym13.
- [38] T. Dahlberg *et al.*, “3D printed water-soluble scaffolds for rapid production of PDMS micro-fluidic flow chambers,” *Scientific Reports*, vol. 8, no. 1, Dec. 2018, doi: 10.1038/s41598-018-21638-w.
- [39] E. Gkartzou, E. P. Koumoulos, and C. A. Charitidis, “Production and 3D printing processing of bio-based thermoplastic filament,” *Manufacturing Review*, vol. 4, 2017, doi: 10.1051/mfreview/2016020.
- [40] D. M. Sánchez, M. de la Mata, F. J. Delgado, V. Casal, and S. I. Molina, “Development of carbon fiber acrylonitrile styrene acrylate composite for large format additive manufacturing,” *Materials and Design*, vol. 191, 2020, doi: 10.1016/j.matdes.2020.108577.
- [41] S. Yuan, J. Bai, C. K. Chua, J. Wei, and K. Zhou, “Material evaluation and process optimization of CNT-coated polymer powders for selective laser sintering,” *Polymers (Basel)*, vol. 8, no. 10, 2016, doi:

10.3390/polym8100370.

- [42] H. Korhonen *et al.*, “Fabrication of graphene-based 3D structures by stereolithography,” *Physica Status Solidi (A) Applications and Materials Science*, vol. 213, no. 4, pp. 982–985, Apr. 2016, doi: 10.1002/pssa.201532761.
- [43] B. Li, L. Zhang, and B. Yang, “Grain refinement and localized amorphization of additively manufactured high-entropy alloy matrix composites reinforced by nano ceramic particles via selective-laser-melting/remelting,” *Composites Communications*, vol. 19, 2020, doi: 10.1016/j.coco.2020.03.001.
- [44] Z. Zhou, I. Salaoru, P. Morris, and G. J. Gibbons, “Additive manufacturing of heat-sensitive polymer melt using a pellet-fed material extrusion,” *Additive Manufacturing*, vol. 24, 2018, doi: 10.1016/j.addma.2018.10.040.
- [45] Bharti *et al.*, “Theories and models of supercapacitors with recent advancements: impact and interpretations,” *Nano Express*, vol. 2, no. 2, p. 022004, Jun. 2021, doi: 10.1088/2632-959x/abf8c2.
- [46] Q. Chang, “Electrical Properties,” *Colloid and Interface Chemistry for Water Quality Control*, pp. 79–136, Jan. 2016, doi: 10.1016/B978-0-12-809315-3.00007-4.
- [47] P. Sharma and T. S. Bhatti, “A review on electrochemical double-layer capacitors,” *Energy Conversion and Management*, vol. 51, no. 12, pp. 2901–2912, Dec. 2010, doi: 10.1016/j.enconman.2010.06.031.
- [48] Bharti *et al.*, “Theories and models of supercapacitors with recent advancements: impact and interpretations,” *Nano Express*, vol. 2, no. 2, p. 022004, Jun. 2021, doi: 10.1088/2632-959x/abf8c2.
- [49] W. Li *et al.*, “Printing assembly and structural regulation of graphene towards three-dimensional flexible micro-supercapacitors,” *Journal of*

Materials Chemistry A, vol. 5, no. 31, pp. 16281–16288, 2017, doi: 10.1039/c7ta02041d.

- [50] Z. Wang *et al.*, “Three-Dimensional Printing of Polyaniline/Reduced Graphene Oxide Composite for High-Performance Planar Supercapacitor,” *ACS Applied Materials and Interfaces*, vol. 10, no. 12, pp. 10437–10444, Mar. 2018, doi: 10.1021/acsami.7b19635.
- [51] K. Shen, J. Ding, and S. Yang, “3D Printing Quasi-Solid-State Asymmetric Micro-Supercapacitors with Ultrahigh Areal Energy Density,” *Advanced Energy Materials*, vol. 8, no. 20, 2018, doi: 10.1002/aenm.201800408.
- [52] C. Zhao, C. Wang, R. Gorkin, S. Beirne, K. Shu, and G. G. Wallace, “Three dimensional (3D) printed electrodes for interdigitated supercapacitors,” *Electrochemistry Communications*, vol. 41, 2014, doi: 10.1016/j.elecom.2014.01.013.
- [53] N. Kim *et al.*, “Highly conductive PEDOT:PSS nanofibrils induced by solution-processed crystallization,” *Advanced Materials*, vol. 26, no. 14, pp. 2268–2272, Apr. 2014, doi: 10.1002/adma.201304611.
- [54] V. Bertana *et al.*, “Rapid prototyping of 3D Organic Electrochemical Transistors by composite photocurable resin,” *Scientific Reports*, vol. 10, no. 1, Dec. 2020, doi: 10.1038/s41598-020-70365-8.
- [55] A. Urrios *et al.*, “3D-printing of transparent bio-microfluidic devices in PEG-DA,” *Lab on a Chip*, vol. 16, no. 12, pp. 2287–2294, 2016, doi: 10.1039/c6lc00153j.
- [56] G. Scordo *et al.*, “Effect of volatile organic compounds adsorption on 3D-printed pegda:Pedot for long-term monitoring devices,” *Nanomaterials*, vol. 11, no. 1, pp. 1–15, Jan. 2021, doi: 10.3390/nano11010094.
- [57] X. Luo, J. Li, and M. Lucas, “Galvanometer scanning technology for laser additive manufacturing,” in *Laser 3D Manufacturing IV*, Feb. 2017, vol.

10095, p. 1009512. doi: 10.1117/12.2252973.

- [58] S. Tang and U. Schulz, “Gas flow sputtering - An approach to coat complex geometries and Non Line of Sight areas,” *Surface and Coatings Technology*, vol. 204, no. 6–7, pp. 1087–1091, Dec. 2009, doi: 10.1016/j.surfcoat.2009.08.016.
- [59] S. Zhang and N. Pan, “Supercapacitors performance evaluation,” *Advanced Energy Materials*, vol. 5, no. 6. Wiley-VCH Verlag, Mar. 01, 2015. doi: 10.1002/aenm.201401401.
- [60] G. A. M. Ali, Z. H. Bakr, V. Safarifard, and K. F. Chong, “Recycled Nanomaterials for Energy Storage (Supercapacitor) Applications,” in *Topics in Mining, Metallurgy and Materials Engineering*, 2021. doi: 10.1007/978-3-030-68031-2_7.
- [61] D. Boonpakdee, C. F. Guajardo Yévenes, W. Surareungchai, and C. La-O-Vorakiat, “Exploring non-linearities of carbon-based microsupercapacitors from an equivalent circuit perspective,” *Journal of Materials Chemistry A*, vol. 6, no. 16, 2018, doi: 10.1039/c8ta01995a.
- [62] B. A. Mei, O. Munteshari, J. Lau, B. Dunn, and L. Pilon, “Physical Interpretations of Nyquist Plots for EDLC Electrodes and Devices,” *Journal of Physical Chemistry C*, vol. 122, no. 1, pp. 194–206, Jan. 2018, doi: 10.1021/acs.jpcc.7b10582.
- [63] C. Shen, S. Xu, Y. Xie, M. Sanghadasa, X. Wang, and L. Lin, “A Review of On-Chip Micro Supercapacitors for Integrated Self-Powering Systems,” *Journal of Microelectromechanical Systems*, vol. 26, no. 5, pp. 949–965, Oct. 2017, doi: 10.1109/JMEMS.2017.2723018.
- [64] S. H. Park, G. Goodall, and W. S. Kim, “Perspective on 3D-designed micro-supercapacitors,” *Materials and Design*, vol. 193. Elsevier Ltd, Aug. 01, 2020. doi: 10.1016/j.matdes.2020.108797.